Paper L

CRATERING FROM A MEGATON SURFACE BURST*

H. L. Brode and R. L. Bjork

The RAND Corporation

Santa Monica, California

ABSTRACT

Assuming a hydrodynamic model, the authors have calculated the stresses and early motions associated with the cratering of a rock medium (tuff) from a 2-megaton surface burst. The results demonstrate the basically two-dimensional geometry of such an explosion, and offer preliminary values of the pressures and motions involved. The excavating action is found to be associated with the direct shock from the bomb, and not due to the loading developed by the air overpressures in the early fireball. A limited description of the method, inputs, and equation of state of rock is included. Graphical results, together with some discussion of the salient features and the various physical assumptions and limitations associated with the calculations make up the body of this report.

* * *

I. INTRODUCTION

The cratering action of large-yield explosions is an important part of both peaceful and warlike applications of nuclear weapons effects. It is a dominant feature in any earth-moving application, such as in the proposed harbor and canal digging (Plowshare) operations. In protective construction for the military, the crater boundaries define a sensible if perhaps extreme limit inside which survival cannot be expected. For an increasing number of applications more exact knowledge of expected craters and the associated ground shocks has become a vital factor.

* This work was sponsored by the U. S. Air Force and supported in part by the U. S. Atomic Energy Commission.

An improved understanding of cratering must come from theoretical work coupled with field work using scaled or small-yield explosions. Ideally, theory and experiment should be combined at the yields of interest, but for several overriding reasons, no large-yield surface (or shallow-buried) bursts have been shot or are contemplated in a site of dry soil or rock, and it is necessary to rely on extrapolation from small nuclear shots and from chemical explosive work for the experimental aspects. Without benefit of adequate theoretical work, the extension of small-yield field data to large-yield situations is at best approximate and at worst may be quite wrong. A clear physical basis for predictions and scaling is particularly desirable at this time, and it is toward that goal that the calculations covered in this report were aimed.

In constructing a reasonable theoretical model of the cratering action, several factors stand out as being immediately necessary: Since the early phases of either chemical or nuclear explosions involve pressures far in excess of the shear or viscosity stresses characteristic of any natural materials, and since the resulting strong shocks induce appreciable compression and heating in the surrounding matter, a hydrodynamic model is not only reasonable but is a necessity at early stages. Furthermore, since the geometry of the burst relative to the interface separating ground and air figures dominantly in the formation of any crater, the hydrodynamics must be carried out in two space dimensions, i.e., must include vertical and radial motions. A program for numerical computation of hydrodynamic motions in two dimensions has existed at RAND for some time, and is particularly appropriate for use on the nuclear cratering problems. The scheme was originally generated by Bjork[1] in an investigation of high-speed impact craters in metals. The programming was done by N. J. Brooks.

Although the hydrodynamic assumption is basic to the model, two further features are of importance, if less obviously so. In order to properly follow the cratering action of a surface-burst nuclear explosion, it is necessary to know with considerable precision the early history of a nuclear bomb explosion. The exact amount of energy (and its form) that enters the ground, and how much

energy goes in or out across the surface of the ground at later times, will depend critically on the bomb energetics and the early fireball and air-blast history. Recent detailed calculations by Brode[2] have made easy the definition of initial and boundary conditions to approximate the influence of the complex dynamic loading induced by a surface-burst nuclear weapon.

One further factor of prime importance involves the equation of state of the earth material. A cratering problem is sensitive to the relation between energies and sound speeds in the two media on either side of the interface. In the air above, the ambient sound speed is about 330 meters/sec, while seismic velocities in natural earth materials vary from typical soil seismic speeds around 600 meters/sec to a speed in granite near 3700 meters/sec. Air is quite compressible and very heat-absorbent at the high pressures in a nuclear explosion, while solid materials are much less compressible and tend to be much less dissipative at comparable stress levels. The extent to which these inequalities matter in such a cratering calculation can easily be appreciated.

As the stress in the soil or rock sinks below a level where hydrodynamics can properly be considered the dominant force in producing motions and transporting energy, the calculation should embrace such physical features as plasticity and elasticity and should then deal with real solid-state features of the material. Although something of this sort has been done in the simpler case of spherically symmetric explosions by Nuckolls,[3] it was not attempted in any comparable sense here in connection with the two-dimensional cratering calculations. Furthermore, since the forces far exceed the force of gravity in the pressure regime where the model is considered valid, gravitational forces were not carried in this program.

II. NUMERICAL METHOD

The motion of the ground itself is assumed to be governed by the compressible, hydrodynamic equations. Written in terms of Eulerian variables, these are

$$\rho \frac{\partial \bar{u}}{\partial t} + \rho \bar{u} \cdot \text{grad } \bar{u} + \text{grad } P = 0 \qquad (1)$$

$$\frac{\partial \rho}{\partial t} + \bar{u} \cdot \text{grad } \rho + \rho \text{ div } \bar{u} = 0 \qquad (2)$$

$$\rho \frac{\partial e}{\partial t} + \rho \bar{u} \cdot \text{grad } e + P \text{ div } \bar{u} = 0 \qquad (3)$$

$$P = P(\rho, e) \qquad (4)$$

where the variables are

$\bar{u}$ particle velocity
P pressure
e specific internal energy
ρ density
t time.

The effects of viscosity and heat conduction are neglected in the above equations. It is possible to show by order-of-magnitude arguments that neglecting heat conduction is a good approximation. However, not enough is known of the viscous properties of materials under high pressures and densities to make such a positive statement relative to neglecting viscosity. Viscosity is really omitted from the framework of these calculations for the practical reason that no good estimates of it are available.

The nature of the problem renders the solution of these equations particularly difficult. Portions of the ground suffer large distortions, so that a Lagrangian description fails after a short time. The Eulerian formulation suffers from the continual diffusion across interfaces.

The numerical technique employed was one previously developed by Bjork[1] to treat problems of high-velocity impact, where similar difficulties occur. Briefly, the method treats mass points moving through an Eulerian mesh. Integration is carried out on time, starting from the initial conditions (described in Section III) and imposing the appropriate boundary conditions. The advance over Δt is carried out in two steps. In the first step, the

transport terms in Eqs. (1) through (4) are neglected, and the integration is performed by solving the difference analog of the resulting differential equations. In the second step, the transport terms are accounted for by noting which masses changed cells in the first step.

To get the new mass of the cells affected, one merely sums the masses now present in each cell, which accounts for the mass transport term in Eq. (2). A mass which changes cells is assumed to carry with it an increment of internal energy given by the product of the mass in question and the specific internal energy of the cell which it left. This accounts for the internal energy transport term in Eq. (3).

A mass, in changing cells, also brings with it an increment of momentum given by the product of the mass and the velocity present in the cell which it left. This momentum is added to the cell entered by the mass, and that cell is given a new velocity equal to the new momentum divided by the new total mass. Thus the momentum transport term of Eq. (3) is taken into account.

The process described conserves mass, internal energy, and momentum. However, it is easily shown that kinetic energy is always lost in this repartitioning unless the velocities of the two cells involved are equal. This is accounted for by arbitrarily adding the loss in kinetic energy of the two cells to the internal energy of the entered cell. Thus, total energy is conserved, but a small fraction of the kinetic energy is converted to internal energy in the process. This conversion may be shown to be equivalent to an artificial viscosity of the Landshoff type,[4] and its presence precludes the necessity of adding any further artificial viscosity to the problem.

In both the previously treated impact problems and the present ground motion calculations, the magnitude of the viscosity is ideal in the sense that it spreads the shock jumps over about three mesh spaces.

The method was tested in two ways. The first was to compare the solution generated for one-dimensional impacts with analytical solutions which are available in this case. This test showed that the method gave correctly the jumps in pressure, density, and velocity across a shock, and also the velocities of the shocks themselves. This means that the jump in entropy

across the shock is given correctly, placing the final state on the Hugoniot rather than the adiabat connecting the initial and final states.

The second test was to calculate with this two-dimensional code a spherically symmetric nuclear air burst previously calculated by Brode[5] with a one-dimensional code. The agreement was checked in the vertical direction, the horizontal direction, and at an angle of 45° between the two, and found to be satisfactory in all cases.

The calculations were performed by an IBM 704 which possessed a 32,000-word fast memory. The memory size was the limiting factor in the resolution. In order to obtain an adequate mass resolution, 20 mass points per cell were used. This meant that on the average a cell's density could change in 5% increments. This choice of the number of mass points restricted the number of space grid points to 400, which were arranged in a 20 by 20 rectangular array. Using fewer mass points per cell would have resulted in a larger number of space grid points, but it was not deemed feasible to coarsen further the mass resolution.

By an artifice known as "grid changing," the 400 grid points were always arranged to encompass only the region of activity and its immediate environs. In a "grid change," the points were laid down in such a manner as to encompass the shock front plus about an equal extent of undisturbed media. Within the shock, the dependent variables were given the values existing at the end of the previous grid, and outside they were assigned values appropriate to the undisturbed media. The new grid was then used until the program detected the first faint movement on the grid's boundary caused by the approaching shock, at which time a new grid change was effected.

In the present calculation, it is possible to gain only a very rough idea of the crater dimensions, as the forming crater is covered only by very few space grid points. The reason for this is that the ground shock is several times as deep as the crater bottom and the grid spacing is uniform in the vertical direction. In this sense the present calculation emphasizes the information relative to the deep ground motion. It will be possible to emphasize the cratering information by using a gradation of grid sizes in the vertical direction, so that there will be many points near the surface and only a few deep underground.

III. INITIAL AND BOUNDARY CONDITIONS

The problem to which we address ourselves is that of calculating the crater and ground motion due to a 2-megaton surface burst. The nature of the problem is contained in the specification of the boundary conditions. These initial and boundary conditions were based on results of calculations by Brode[2] of the early phases of a nuclear explosion. From these calculations at 1 microsecond after initiation, one finds that approximately half the bomb energy has radiated out of the bomb into the surrounding air, and most of the energy remaining in the bomb is in directed kinetic energy of the bomb materials. At this time it is reasonable to characterize the explosive input to the ground as due to both the impact of the bomb mass on the ground directly below it and to the pressure on the surface from the initially extended and rapidly growing fireball or strong shock in air. The pressures generated by this air blast are initially several orders of magnitude less than the pressures created directly by the bomb vapors, since the energies in the air and in the bomb are comparable, but the volume of air is many times larger than that occupied by the bomb itself.

These initial conditions lead to a specification of velocities of the order of 1700 m/ms in the first few zones of the rock, representing the mass and kinetic energy of the lower half of the bomb. In these zones an appropriate internal energy was included. These conditions, together with the initial choice of grid spacings, lead to the following initial configuration:

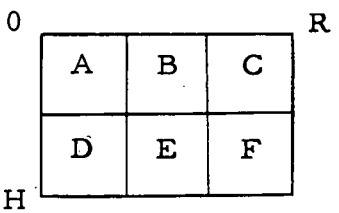

In the grid, each initial zone was 1/4 meter both across and deep, representing rings of mass in the cylindrical coordinates used. Each of the six "bomb" zones had a specific internal energy (and a pressure associated with it) corresponding to 8.05×10^5 in the meter-millisecond-megagram system

of units used here (i.e., in 10^{16} ergs/10^{6} gm). Each of these zones also had an initial velocity of 1670 m/ms, directed radially, so that the initial velocity components were as in Table 1.

Table 1

	Vertical Velocity V	Horizontal Velocity U	E	ρ_0
A	1181	1181	8.05×10^5	1.7
B	528	1584	"	"
C	327	1638	"	"
D	1584	528	"	"
E	1181	1181	"	"
F	859	1432	"	"

Energies, pressures and velocities were all initially zero outside of the six bomb zones. These bomb zones represented only the lower half of the bomb in a "true" surface burst position (i.e., with the center of gravity located on the plane of the surface between rock and air). The upper half of the bomb had been carried in the calculations in an early version, but proved to have an entirely negligible effect on the subsurface behavior. Since it added to the complexity of the problem to follow the upper masses as they flew off at high velocity, they were omitted from subsequent computations.

The surface pressures due to the air blast were included in the form of a boundary condition on the uppermost masses. An analytical form representing the air pressures as a function of time and radius was developed from the detailed calculations of an air-burst megaton explosion.[2] The fit is approximately correct from earliest times until around half a second, after which it increasingly overestimates the pressures. At half a second the peak overpressure in the air shock should be about 145 psi (at a shock radius of more than one kilometer) while the fit gives about 180 psi. A comparison

between the detailed calculation overpressures and the fit used is made in Fig. 1. The impulse from this overpressure in its positive phase is generally too high by a factor of 1.5 over the applicable range of distances. Since nearly all of the observed ground motions were directly attributable to the direct impulse from the bomb vapors and not at all from the air blast impulse, the use of an air overpressure formula which overemphasizes the air impulse is conservative in the present calculations, and emphasizes that no appreciable change would have resulted had the air overpressure been completely ignored.

The formula employed for the air overpressure boundary condition is the following:

$$\Delta P = \frac{0.62}{0.1 + t^{1.15}} \left[1 + 1.6\left(\frac{t_s}{t}\right)^6\right] 10^{10} \text{ dyne/cm}^2$$

where t_s is the time of shock arrival, t is the time (both in milliseconds), and $t \geq t_s$.

$$t_s = 7 \times 10^{-5} + 7.24 \times 10^{-20} R_s^{10}, \text{ for } R_s \leq 56,$$

$$= \frac{7.24 \times 10^{-20} R_s^{10}}{1 + 0.637 \times 10^{-14} R_s^{7.5}}, \text{ for } 56 < R_s < 200,$$

$$= \left(\frac{R_s}{95}\right)^{2.5}, \text{ for } R_s \geq 200 \text{ m},$$

in which R_s is the shock radius in meters. At times before shock arrival the overpressure is zero.

For a low air burst, in which the bomb materials do not get close enough to the ground to shock it strongly, the main mechanism for inducing ground motion would be just the air blast. The above form could also represent the approximate pressure history on the surface from a burst at about 100 meters above the surface. At that burst height the direct bomb shock would be

negligible, but the air shock would be quite similar to that from a true surface burst for horizontal ranges greater than about 100 m.

Since the compressions in the ground from such a low air burst would be quite small, the particular numerical scheme used here is not appropriate. It may be more reasonable to carry out such a calculation using a Lagrangian scheme, more adapted to propagations with small density changes. It is fairly clear that the nature of the air-slap loading is such that no conventional crater will occur from it alone in rock or in most soils. Its load is applied so rapidly over such a wide area and is relieved so rapidly that the main response is a tendency to compact, and very little excavating motion would be generated. On the other hand, the induced ground shock will not be entirely in the vertical direction, and will be quite divergent, i.e., will not be a plane wave. These trends as stated here were substantiated by two calculations which used only the air-slap input. Unfortunately these same calculations used unreal equations of state, and so are not useful beyond their indications of a general geometric nature.*

IV. EQUATION OF STATE

The influence of the equation of state on the results of such calculations has been only partially explored. A preliminary problem using an ideal gas of specific heat ratio three ($\gamma = 3$) was run, but at the lower pressures it suffered most from the fact that the computation treated all shocks as strong shocks. In the region where the ground shock is properly strong, the comparison with a more nearly correct equation of state shows an expected greater effective explosion energy for the ideal gas case. Since, for real gases, much more energy is involved in the ionization and dissociation of the hot gas behind

* The first was an ideal gas, strong shock case, and the second used an unusually "soft" fluid. The second problem was not restricted to the strong shock limitation and did have a reasonable seismic speed (~2000 ft/sec), but was too compressible to be realistic. (A pressure of 20 Kbars would cause a compression to twice the original density.) A more appropriate problem will be carried out soon.

the shock front, the shock in a real gas very quickly drops to a lower strength than the corresponding shock in an ideal gas of high specific heat ratio.

The best equation of state used so far represents a soft volcanic rock called tuff (the rock in which some underground nuclear explosions at the Nevada test site were shot). This equation of state was represented by an analytical formula fitting three general regions of information. At the high-temperature end, the fit was to data from a Fermi-Thomas-Dirac calculation for an appropriate mixture of elements representing the chemical constituents of tuff. We are indebted to Bill McMillan of RAND for this data, and to Forrest Gilmore and Arthur Smith of RAND for some thermodynamic interpretation. In the region between 80 and 300 kilobars, the Hugoniot data from high explosive experiments on tuff were used as guidance for the fitting. These data were a part of experimental work carried out by a group at the Livermore Laboratory of the AEC, and were called to our attention by Arthur Smith.

In carrying the fit to lower pressures, the observed speed of sound in tuff was used as a limiting condition. The fit, while only approximately satisfying all of these restrictions, is considered compatible with the accuracy limits imposed by other physical approximations involved in the calculations.

Expressed in terms of the specific internal energy (E) and the density relative to the standard density for tuff ($\eta = \rho/\rho_0$), the pressure, according to the resulting fit, was defined as

$$P = 0.425\eta E + 0.113\eta^{3/2}E + 5.30\eta E^{1/2} + 0.707\eta E^2/(10^5 + E),$$

P in 10^{10} dyne/cm^2,

E in 10^{10} erg/gm,

$\eta = \rho/\rho_0$,

$\rho_0 = 1.7$ gm/cc.

Of course, the solid state properties of the rock which become important at stress levels below about 10 Kbars are not realistically covered by the concepts of thermodynamic equilibrium implicit in the equation of state. But further, the above equation includes no special consideration for phase

changes — melting and vaporizing. It appears unlikely that the inclusion of phase changes would cause the equation-of-state behavior to be radically different from that assumed, however. In the first place, both the melting and vaporization points occur in about the same temperature range, and neither would occur at a precise temperature but would be spread over a factor of two or so in temperature. It is questionable that a melting point would even exist under explosive loading. The shock pressure at the melting temperature should be somewhat less than 100 kilobars, and the above fit covers this region by bridging smoothly the gap between Thomas-Fermi-Dirac results and high-explosive experimental results.

Tuff is a rock which contains an unusually high amount of voids. It is not likely that the collapse of the voids creates a permanent change in the tuff density at the high pressures, since at the highest temperatures the material is violently excavated, and at more modest temperatures (near melting) the voids seem to reconstitute themselves. At the lowest stress levels (below 10 Kbars) where this hydrodynamic model is already inapplicable, permanent void collapsing is likely. No such hysteresis was included in the treatment here. The equation of state for tuff used in these calculations is graphically illustrated in Fig. 2.

V. THE RESULTS

Although the boundary and initial conditions specified accurately both the bomb-vapor residual energies and the impulse from the air-blast slap, it is a striking feature of the results that only the former plays an important role in the excavation process. The air slap does indeed send a shock into the ground, but over a wide area and at pressures several orders of magnitude less than those at the same time in the direct bomb shock. Out along the surface beyond the region of the crater, of course, the air-blast slap exceeds the direct shock (which arrives later), but for the cratering action, and for shocks immediately below the crater, one could validly omit the air slap.

In Fig. 3, the early pressure field is displayed as a map of isobars (at 0.1026 ms). The bomb shock has created a nearly hemispheric shock front

with peak pressures of around 7000 Kbars in the 90° solid angle downward about the vertical axis (darkened area). The lack of a sharp front to the shock at this stage is due to the nature of the computation scheme which spreads shock discontinuities over about three zones of the chosen space grid. Such spreading does not seriously affect the Hugoniot or shock values of the various hydrodynamic variables. At this time, about one-tenth of a millisecond, the direct shock has progressed only some 7 meters, while the air shock aided by radiation diffusion has gone out more than 50 meters. The 7-megabar ground shock pressures are to be compared with the peak overpressure in the air shock at this time of some 30 kilobars. The shaded box at the origin represents the volume of rock in which the initial kinetic and internal energy was put, to approximate the bomb. It is already clear at this time that the ground shock is no longer dependent on the geometrical details of the source.

Figure 4 displays the velocity vectors of various rock masses at this same early time. Here the symmetrical nature of the strong shock generated by the bomb energy becomes even more evident. All the compressed region of the shock front is rapidly expanding spherically. The topmost rock is being blown off into the air (in this case into the fireball above) at extreme velocities. This upward flying rock is of course not a true vapor and is already at fairly low density. The same is true of that material below the surface and well behind the shock front, although the motions are more nearly random below a couple of meters depth.

At 10 times this early time, at 1 millisecond, the shock has advanced to some 18 m deep and has dropped to a peak pressure (in the vertical cone) of the order of 500 Kbars (Fig. 5). The shock front is still fairly uniformly spherical out to 45° from the vertical, dropping an order of magnitude from there to the surface. The pressure behind the shock appears more chaotic.

Later, at 3.4 ms, the shock has progressed down to 32 m and fallen to a peak pressure of around 125 Kbars in the same 90° vertical cone (Fig. 6).

The subsequent progress is illustrated at various times (at about 10, 21, 50, 80, and 100 ms) in Figs. 7 through 14. Throughout these figures one can follow the hemispherical shape of the shock. At all times the peak pressures

along the vertical are largest and extend fairly uniformly out to a point 45° from the vertical before a serious drop in pressure begins as one follows the shock front further toward the surface. At the later times (> 40 ms) the calculation has been illustrated beyond a point where all pressures are below 10 kilobars, and so beyond a time when the hydrodynamic assumption is reasonably rigorous. It is interesting to note that at these late times, when the shock is no longer strong enough to make a fluid of the rock, the velocity maps (Figs. 10, 12, and 14) indicate a fairly sharp cleavage at around 70 m deep. Above that point the material is moving up and continues to go up. Below that depth the material continues to move down. This "crater bottom" persists at the same depth after the 50-ms time. Since this is a fluid model, and since we have claimed no rigor for the model at late times and low pressures, this evidence of a crater depth approximately equal to that predicted by conventional scaling laws[6] can be considered at least in part as a gratifying coincidence. It should be noted, however, that conservation of mass, momentum, and energy in the correct geometry are still appropriate and are in fact responsible for the motions illustrated, and it may well be that the plastic and elastic properties of the rock play secondary roles in determining crater depths.

Pressures as a function of time at fixed vertical positions fairly close beneath the source display the usual strong shock type of bimodal decay in which the pressure, after rising to a peak and falling rapidly for a time, follows a more gradual decay rate (Fig. 15). At greater distance less structure is evident in the pressure histories (Fig. 16), and only rough values of peak stress and total impulse are derivable from them. A similar description applies to the pressure histories at positions along the line inclined at 45° from the horizontal (Figs. 17 and 18), but the pressure-time relations at points along the surface are quite different. Along the surface, air pressures arrive first, dropping from a peak air overpressure (not shown in Figs. 19 and 20) to a "slowly" decaying fireball pressure. Later the direct ground shock arrives, driving the pressure up one or more orders of magnitude for a short time. At distances beyond a few tens of meters (Fig. 20), it is clear that in

surface pressure histories the direct shock rapidly drops out of importance, and at horizontal distances much greater than 100 meters, the direct shock can be ignored. But it does not follow that the direct shock can be ignored at depths below the surface at the same horizontal distances. Referring to Fig. 13, it is evident that the direct shock brings pressures up to 2 kilobars out to a distance larger than 200 meters, but at depth of some 100 meters. Even at a 50-meter depth one would expect 1 kilobar, and perhaps 1/2 kilobar (> 7000 psi) at depths less than 20 meters and at ranges better than 200 meters. At distances much beyond 200 meters, however, and at depths of less than 100 meters (or more nearly correctly, at depths such that a direct line to the point of explosion makes an inclination from the horizontal of less than about 20°), it is the air blast alone which creates the pressure pulse. The peak overpressure from the air blast will be almost an order of magnitude higher than that from the direct shock at 100 meters, while the air blast impulse is already a little larger than the impulse in the direct shock at the surface at that distance.

In Fig. 21, the peak pressures in the direct shock are shown versus the radial distance from the point of burst for the three directions, as solid curves labeled vertical (V), horizontal (H), and diagonal (D). In the early, strong shock region the decay of pressure is approximately as the inverse cube of the distance, while at lower pressures the decay is less rapid, approaching the inverse three-halves power of the radial distance. The pressures along the surface (H) continue to drop rapidly even at large distances, since a rarefaction wave propagates downward from the surface on which the air pressure is at every instant much lower than the vertical ground shock pressures. The air was not always at a lower pressure, since at an earlier time the air shock created surface pressures much higher — about as indicated by the small circles. The dashed curves are from the ideal gas calculation. These begin at higher pressures but continue to drop rapidly at low pressures because of the strong shock restriction involved in the ideal gas calculations. The shock compression in the vertical and horizontal directions is indicated by the curves labeled $10(\eta - 1)$, where $\eta = \rho/\rho_0$. Thus at 10 meters the vertical shock has a density of $2\rho_0$ and the horizontal shock a density of $\sim 1.5\rho_0$.

Figure 22 illustrates the maximum components of velocity as a function of distance down the vertical and also horizontally. From this one observes that the velocities along the vertical are dominantly vertical (V_v) but have some slight radial component (U_v) indicating some hemispherical divergence. The velocities along the horizontal are both upward ($-V_v$) and outward (U_n), and of comparable magnitudes at most distances.

As the problem progressed, and as it was necessary to include more material into which the shock could run, new and larger sets of zones were arranged and the hydrodynamic variables adjusted to the new grid according to the conservation laws. When such new grids were introduced, those masses above the initial surface and having high-speed motions upward were omitted. In excluding these jettisoned materials some energy and mass is lost to the system. Slightly less than 50 kilotons of mass were ejected by this procedure (in the 100 milliseconds covered). (It is estimated that altogether something on the order of megatons of material are carried aloft and tossed out of the crater from such an explosion.) Figure 23 shows this mass loss as a function of time along with the energy changes.

A study of the energy-time relations shown in Fig. 23 leads to the following observations: The downward kinetic energy, initially half a megaton, decreases rapidly as the shock develops in the surrounding rock. The heat or internal energy builds up rapidly at the expense of the initial kinetic energy, but begins to return to kinetic energy as surface material blows off. The sharp drops in energy occur as blown-off masses and their associated energies are eliminated at grid changes. Note (Fig. 23) that the biggest drop is in the kinetic energy. The total energy drops both because of such periodic (and arbitrary) mass losses and because of the work done continuously against the high-pressure air of the fireball above. At the beginning the total energy is 600 kilotons (30% of 2 megatons), but by the time the direct shock is out some 50 m, the energy is down to less than 100 kilotons (< 5%), and must drop further by both mechanisms.

The seemingly strange behavior of the internal energy at late times (Fig. 23) is an unfortunate consequence of the treatment of energies and

pressures at low densities. Although negative pressures were not allowed (replaced as zero) in the calculation, negative internal energies did arise in low-pressure, low-density zones as these zones did work on their surrounding zones. The lack of consistency here is considered to be due to undamped and nearly random kinetic motions which absorb the energy and thus cause it to be recorded as kinetic rather than as internal. It is perhaps only a misidentification which makes the energy partition motions artificial, but it may also be a source of real error since if energies were allowed to become consistent with a simple gas pressure, the pressures might well have been higher, causing further accelerations. This effective transfer of energy did not become seriously "out of line" until times after 10 ms, so that although late-time information may be of doubtful accuracy, the early history should still be correct.

An investigation of ways to avoid this trouble is still in progress, although it is currently expected that the general features of the present calculation will remain unaltered by the correction of this inconsistency.

VI. CONCLUSIONS

Perhaps the most significant result to come out of these preliminary calculations, aside from the general observation that the method seems capable of offering an interpretation of cratering phenomena, is that the kinetic energy in the bomb debris when it reaches the ground is the most important mechanism in inducing the ground motion below the crater, as well as in the formation of the crater itself.

This fact implies that the crater size should be very sensitive to the height of burst near the ground. For if the debris must travel even a short distance through air before contacting the ground, its energy may be seriously reduced as it drives a strong air shock. This energy is quickly radiated away to the periphery of the fireball and contributes to increasing the air blast at the expense of cratering efficiency.

Moreover, it implies that the cratering is sensitive to the details of the bomb disassembly in that this process determines the partitioning of bomb

energy between the debris' internal and kinetic energy and that radiated away to air. This indicates that shallow burial or denser case should enhance cratering efficiency.

It also shows that comparisons with high-explosive bursts in this regime would seem particularly unfruitful, since the early energy partitions between explosive gases, air, and earth are vastly different.

A further remarkable quality is that the presence of a nearly free surface causes the stress patterns below the burst to be elongated along the vertical axis. The fact that the pressures along the shock front are far from uniform at any given time is understandable in terms of the geometry of the surface burst, but was not always a recognized factor in previous analysis of ground shocks generated by nuclear bursts at low heights above the surface, on the surface, or shallowly buried.

A further feature worthy of reiteration is the nature of the continuous loss of effective energy in the ground medium due both to the work done by the expanding ground against air overpressure and to the essential disassociation of jetting material from the main body of soil or rock.

It would appear that further investigations should include studies of

(1) Subsurface bursts.

(2) Bursts in other materials, both hard rock and dry soil. (It may prove interesting to consider some cases of bursts on wet soils or even water.)

(3) High explosive bursts for the sake of comparison and to illustrate more clearly the differences in the action between nuclear and chemical explosions.

(4) Special geometries of high explosive charges with a view to modeling the stress wave history of a nuclear explosion (an investigation of this possibility is currently under study at SRI with DASA sponsorship).

These preliminary calculations were intended to reveal the basic nature of the cratering process and the formation of ground shocks. That the hydrodynamic model was used should always be kept in mind. This limits the strict

applicability of these results to pressures greater than 8 kilobars (which corresponds to compressions of greater than 10%) for the soft rock, tuff, which was the only material considered. It is believed that above this compression and pressure, the results are substantially correct, although the various uncertainties could easily lead to errors of about a factor of two.

Even recognizing this, it is of interest to examine the results of the present model beyond the region of its strict applicability, for it is not unreasonable to expect that at least the first motions are given correctly by it, leading to roughly correct values of peak pressure and peak velocity. However, the energetics at late times are questionable, and are subject to further interpretation.

It is hoped that the results presented here will furnish useful guidance and inputs to further studies at lower stress levels, which are very important to the design of protective structures. At these lower stress levels, the present hydrodynamic model must be replaced by one which considers the tensor nature of the equation of state.

ACKNOWLEDGMENTS

The authors wish to credit Mrs. Nancy J. Brooks of the Computer Sciences Department at RAND with recognition for her truly professional management of the entire computing program of this problem. In addition to her competent organization of the numerical work, Mrs. Brooks participated enthusiastically in discussions and decisions concerning the progress of the overall effort. Our appreciation extends also to Miss Linda Larson, Mrs. Margaret Cohen, and Mrs. Rosemary Plue for aid in the analysis and preparation of report graphs.

Although this study was initiated primarily to satisfy a need in military applications, the method and some results are of significance to several proposals for peaceful uses of nuclear explosions under the Plowshare program of the Atomic Energy Commission. For this reason the study was funded in a small part under Contract No. AT(11-1)-135 with the University of California Lawrence Radiation Laboratory at Livermore, California.

REFERENCES

1. Bjork, R. L., and N. J. Brooks, A Numerical Technique for Solution of Multi-Dimension Hydrodynamic Problems, The RAND Corporation, Research Memorandum RM-2628 (to be published).
2. Brode, H. L., Weapon Effects for Protective Design, The RAND Corporation, Paper P-1951, 31 March 1960.
3. Nuckolls, John, in Proceedings of the Second Plowshare Symposium, Part I: Phenomenology of Underground Nuclear Explosions, University of California Lawrence Radiation Laboratory (Livermore) Rept. UCRL-5675, May 1959, pp. 120-134.
4. Landshoff, Rolf, A Numerical Method for Treating Fluid Flow in the Presence of Shocks, Los Alamos Scientific Laboratory (1955).
5. Brode, H. L., "Numerical Solutions of Spherical Blast Waves," J. Appl. Phys., Vol. 26, No. 6, June 1955, pp. 766-775.
6. Glasstone, S. (Ed.), The Effects of Nuclear Weapons, AEC and DOD, pp. 209-213, June 1957.

/bs

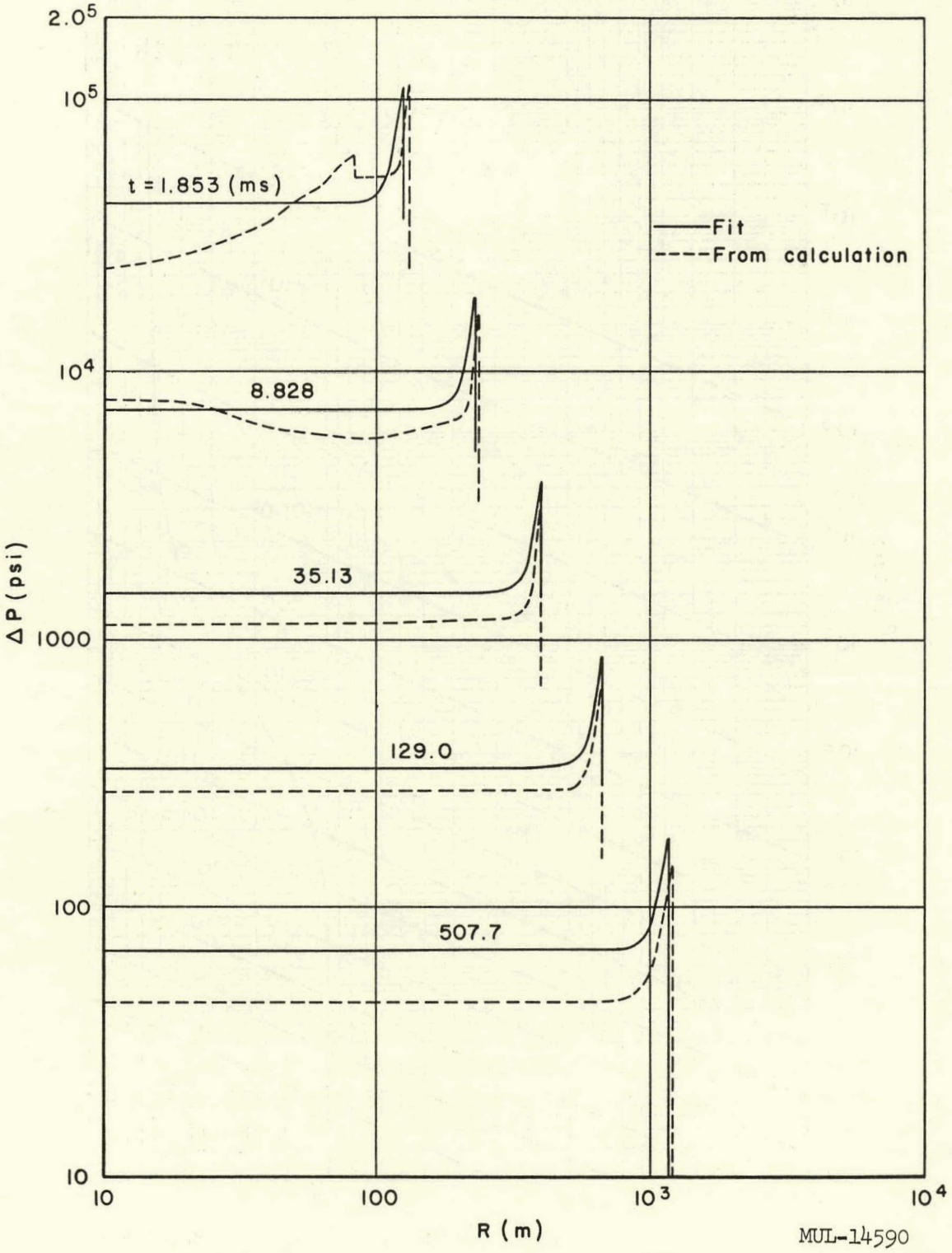

Fig. 1—Comparison of air overpressure approximate analytical form (——) with detailed numerical results (– – –)

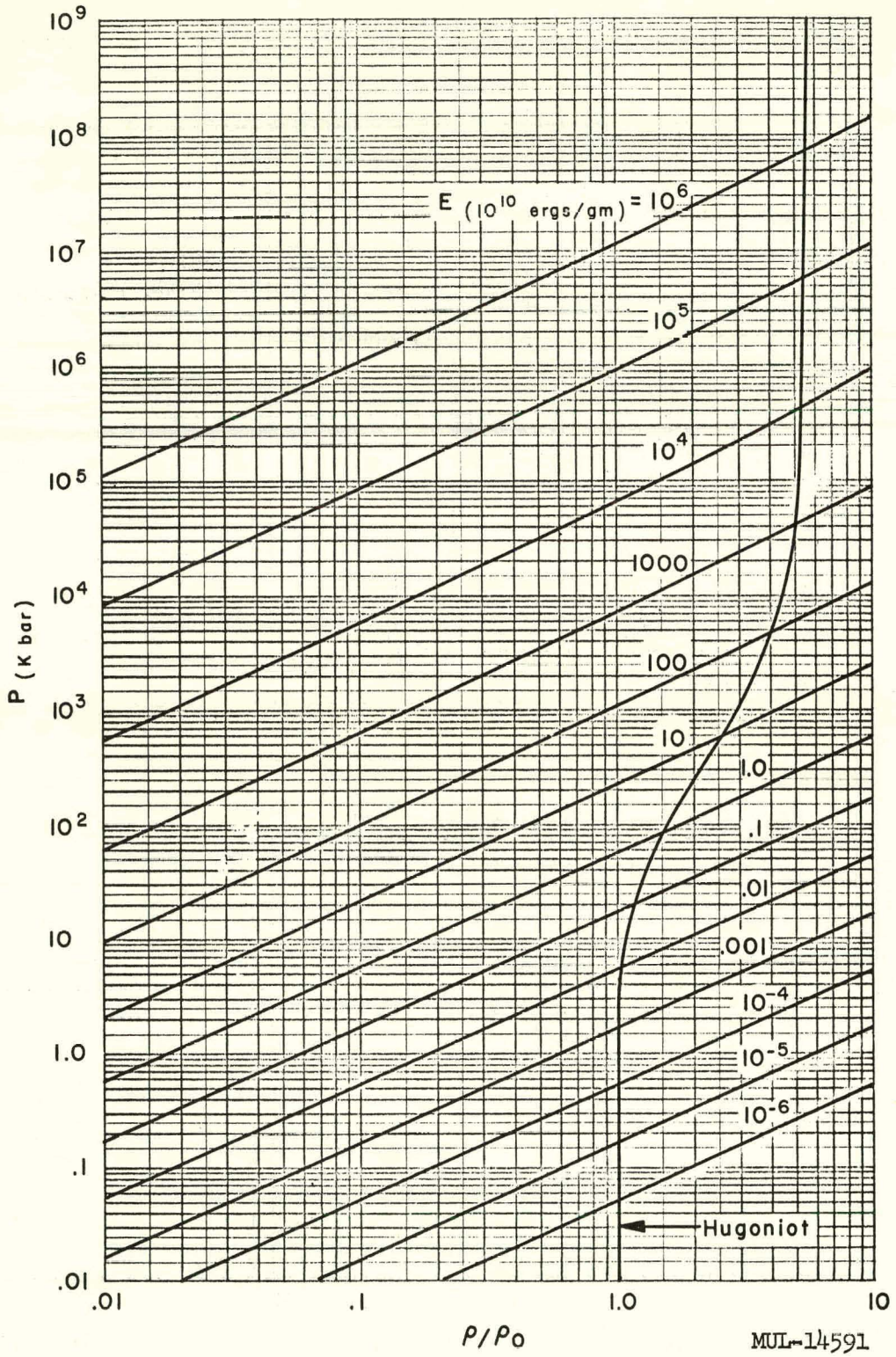

Fig. 2—Equation of state for Tuff

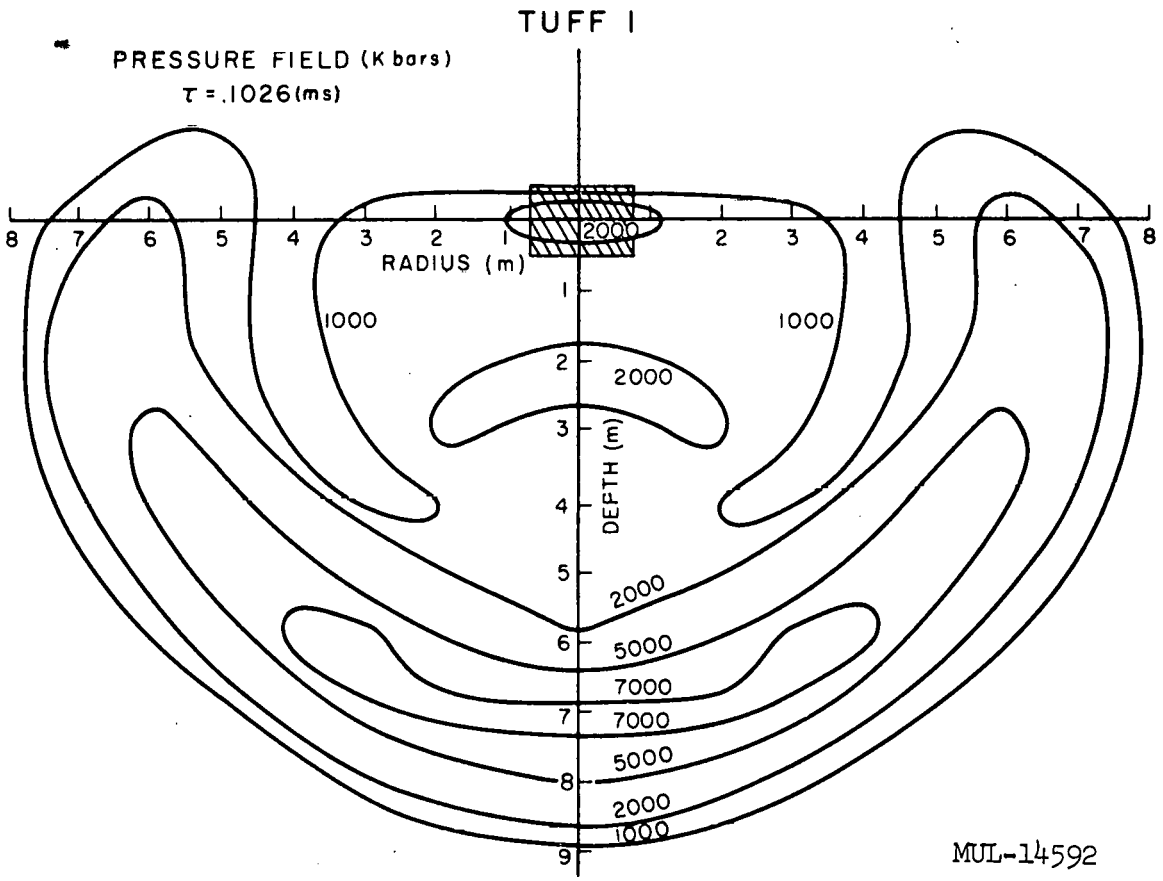
TUFF I
PRESSURE FIELD (K bars)
τ = .1026(ms)
RADIUS (m)
DEPTH (m)
2000
1000
1000
2000
2000
5000
7000
7000
5000
2000
1000
MUL-14592

Fig. 3

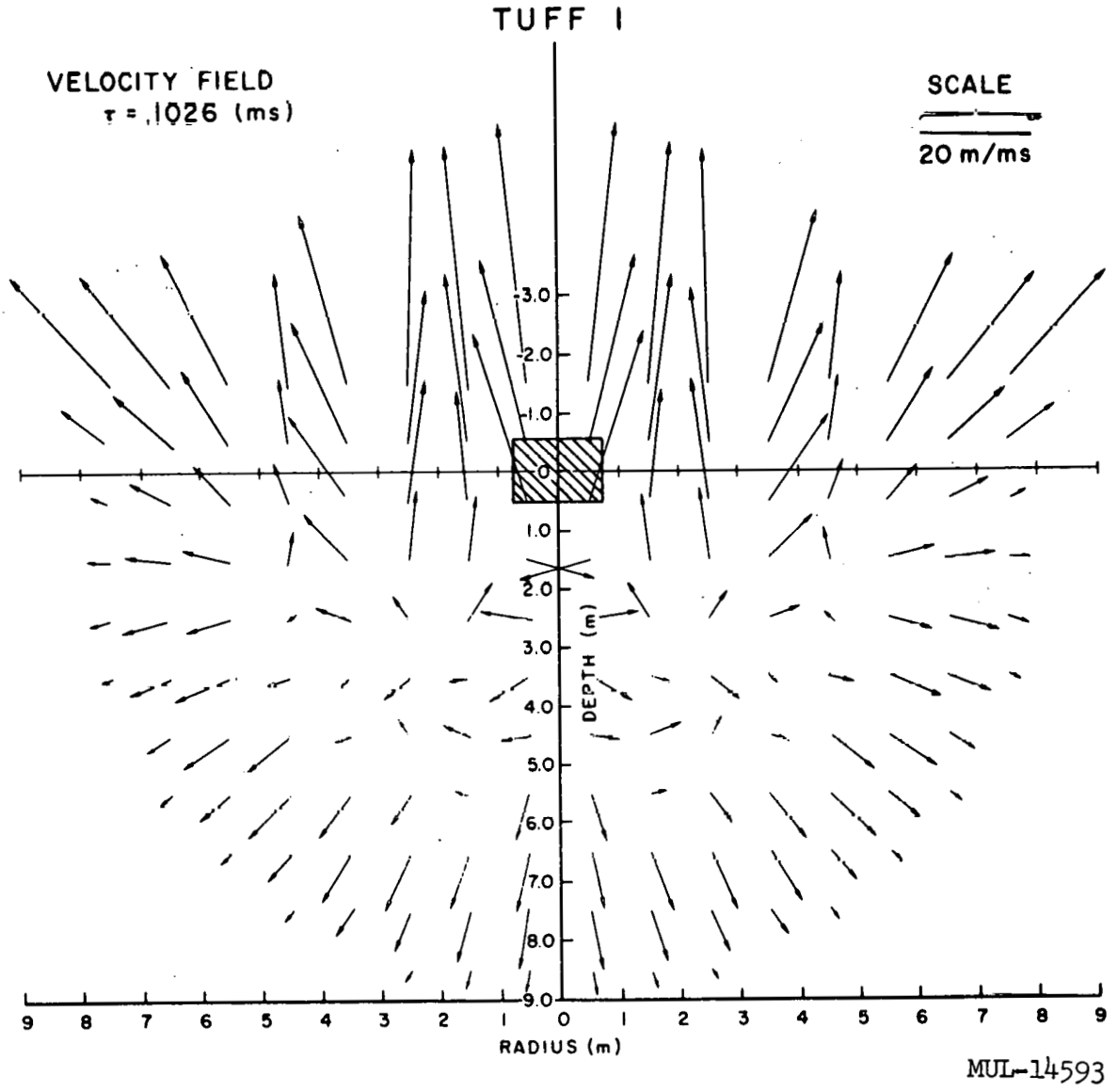
TUFF I
VELOCITY FIELD
τ = .1026 (ms)
SCALE
20 m/ms
DEPTH (m)
RADIUS (m)
MUL-14593

Fig. 4

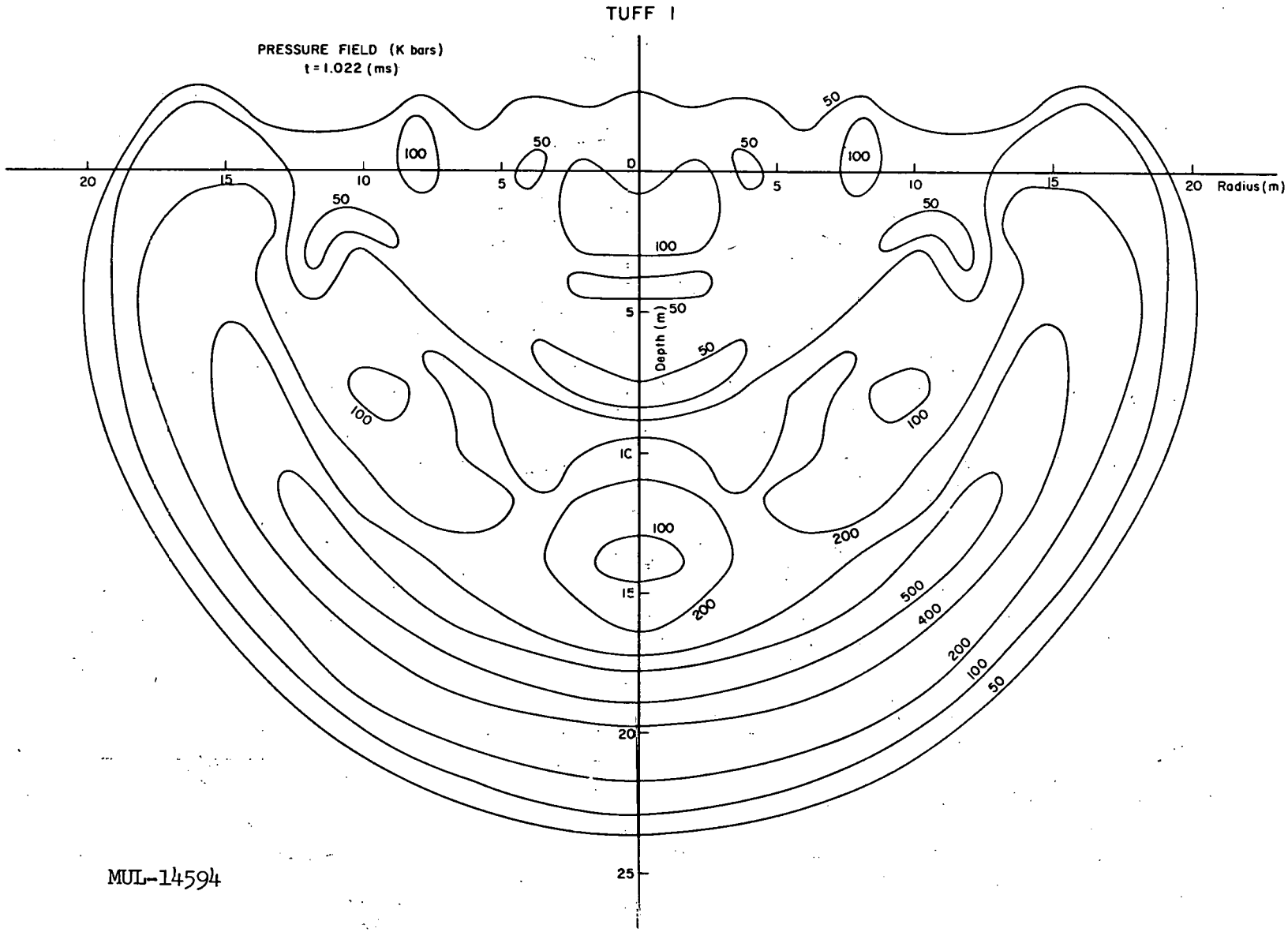
TUFF I
PRESSURE FIELD (K bars)
t = 1.022 (ms)
Radius (m)
Depth (m)
MUL-14594

Fig. 5

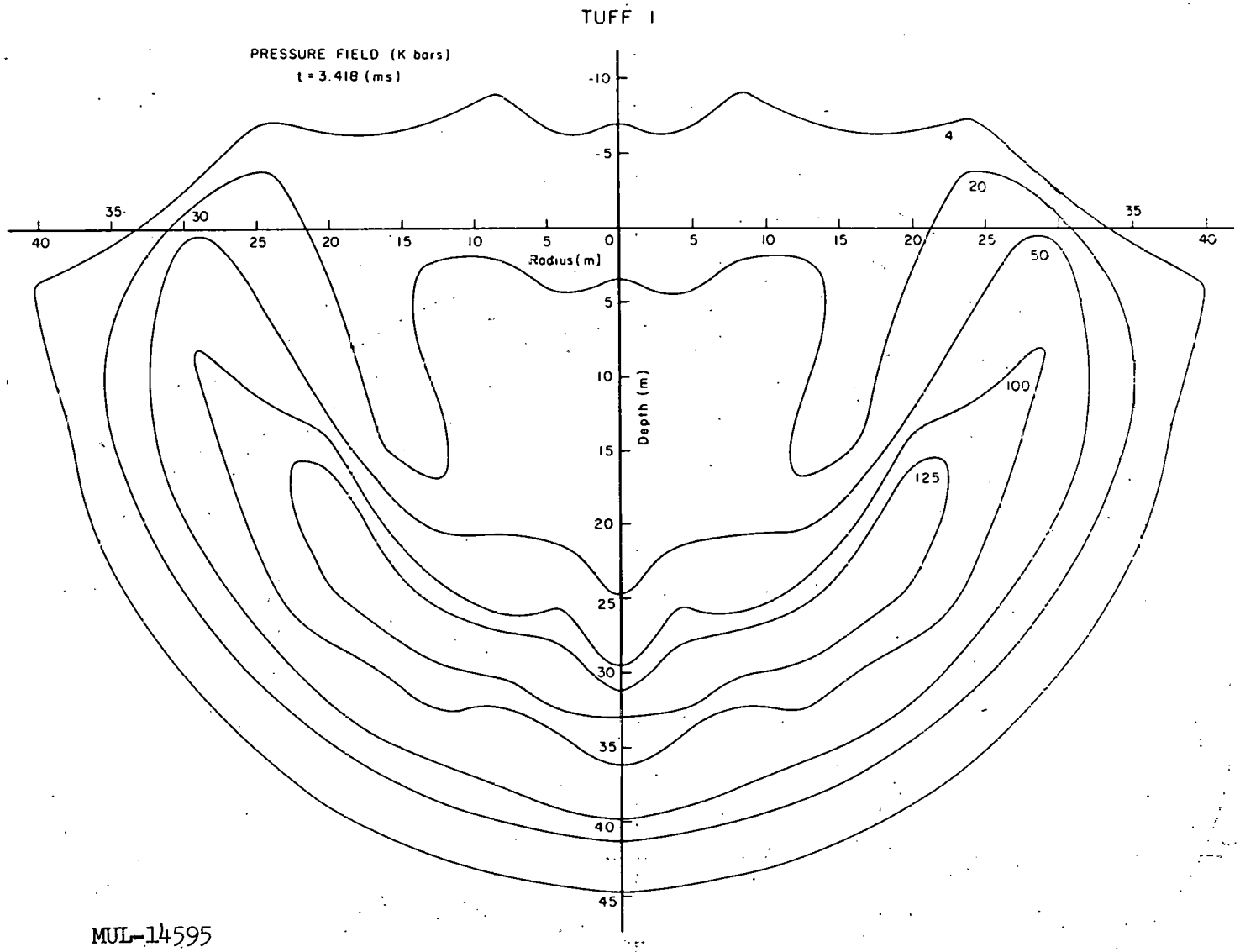
TUFF 1
PRESSURE FIELD (K bars)
t = 3.418 (ms)
Radius (m)
Depth (m)
4
20
50
100
125
MUL-14595

Fig. 6

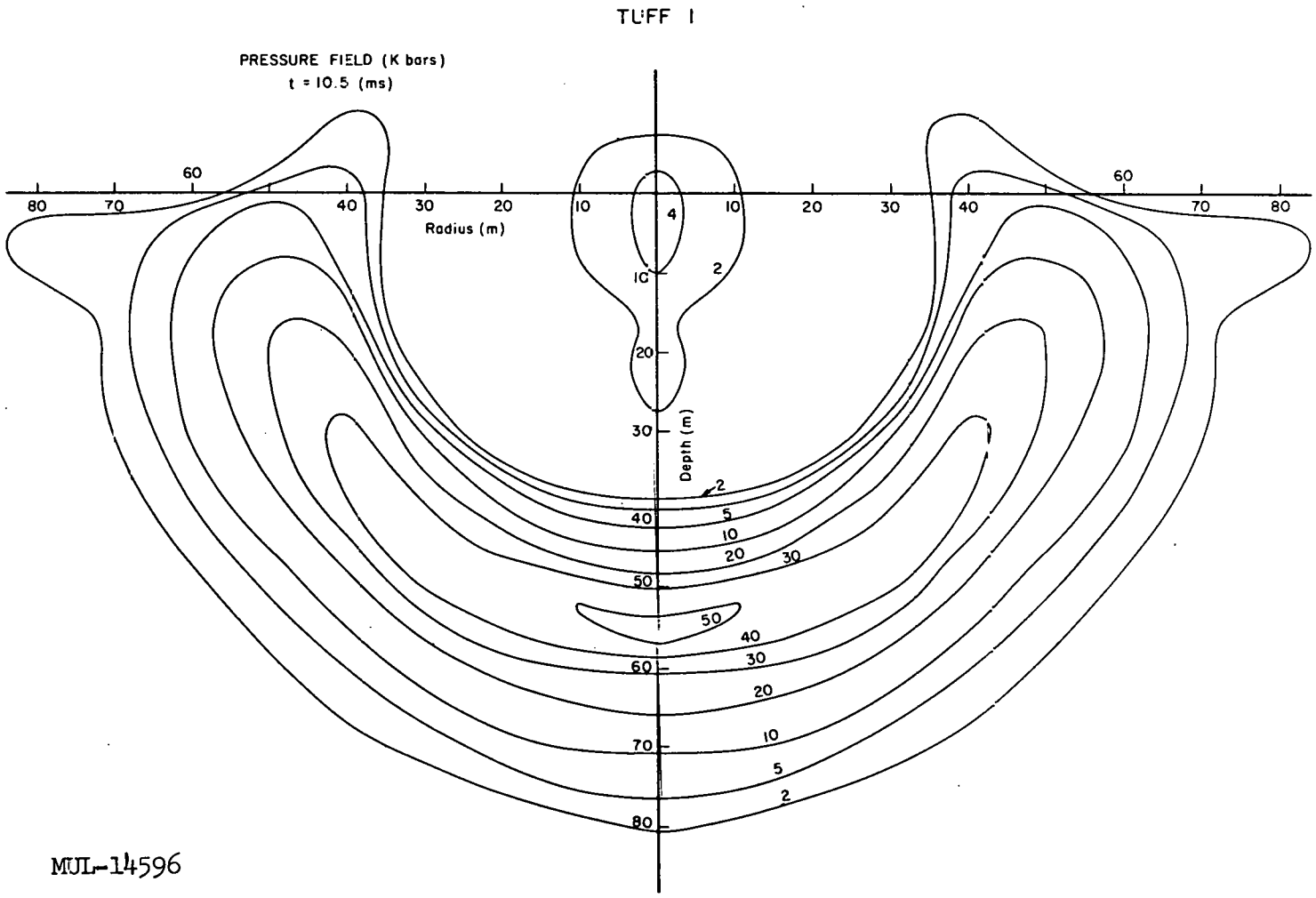
TUFF I
PRESSURE FIELD (K bars)
t = 10.5 (ms)
Radius (m)
Depth (m)
MUL-14596

Fig. 7

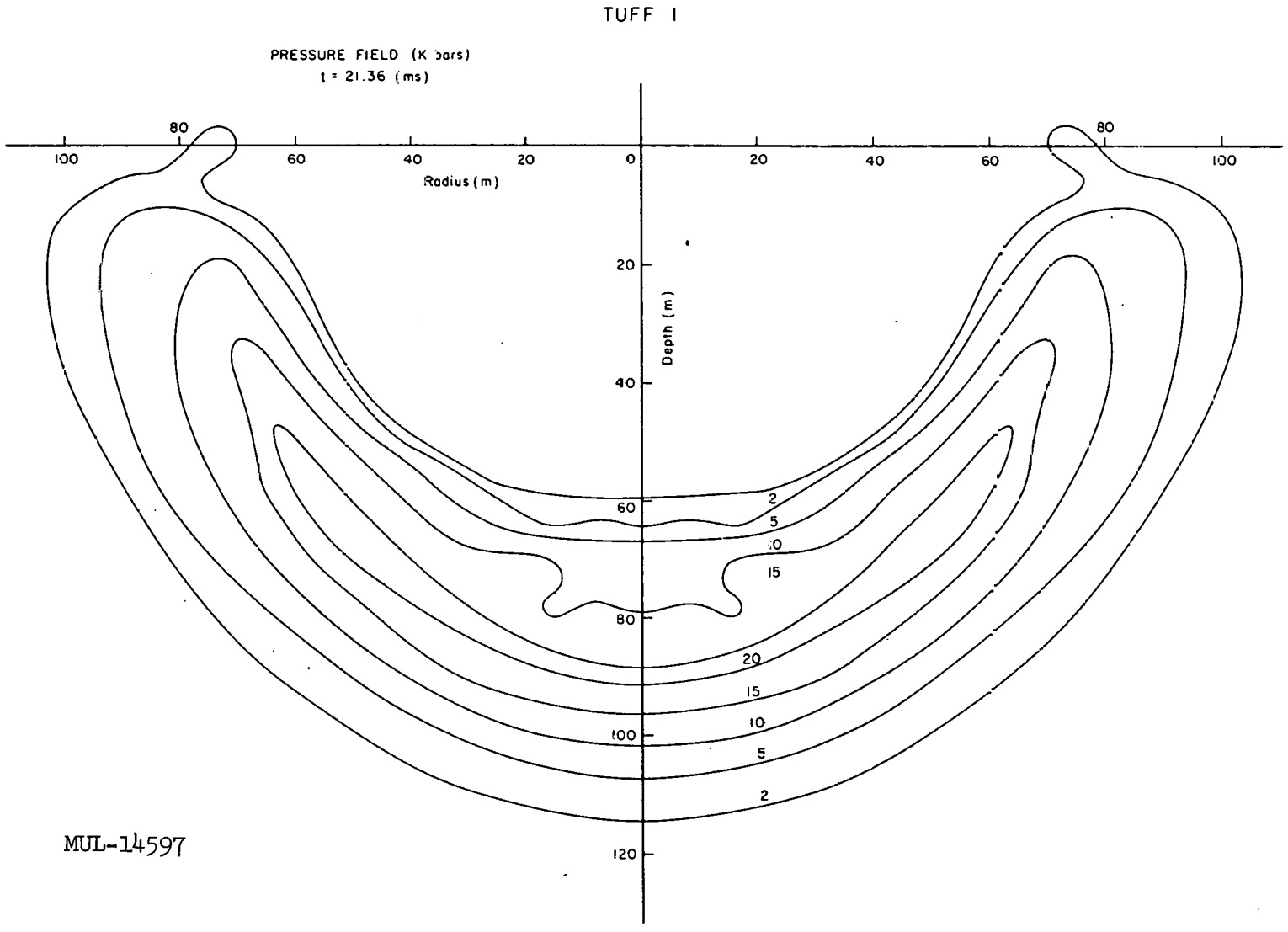
TUFF 1
PRESSURE FIELD (K bars)
t = 21.36 (ms)
Radius (m)
Depth (m)
100
80
60
40
20
0
20
40
60
80
100
120
2
5
10
15
20
15
10
5
2
MUL-14597

Fig. 8

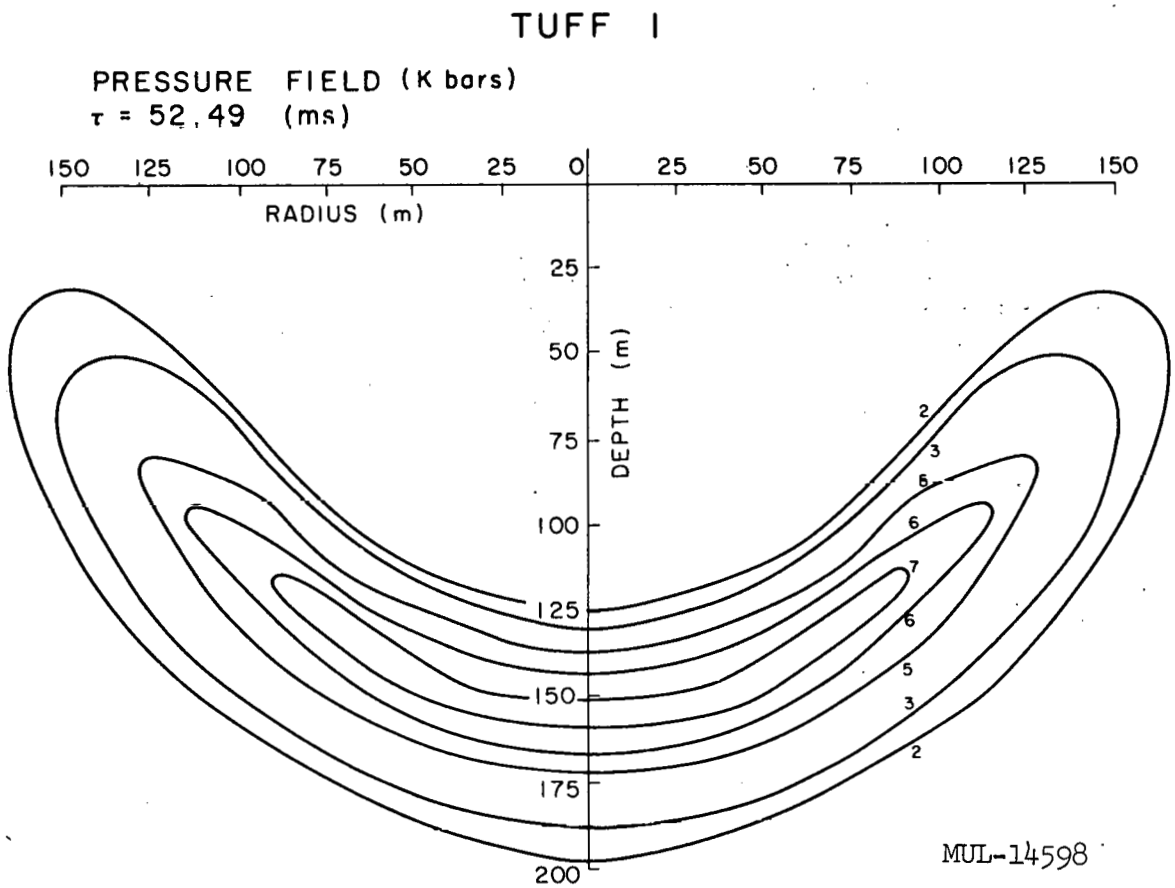
TUFF I
PRESSURE FIELD (K bars)
τ = 52.49 (ms)
150 125 100 75 50 25 0 25 50 75 100 125 150
RADIUS (m)
25
50
75
100
125
150
175
200
DEPTH (m)
2
3
5
6
7
6
5
3
2
MUL-14598

Fig. 9

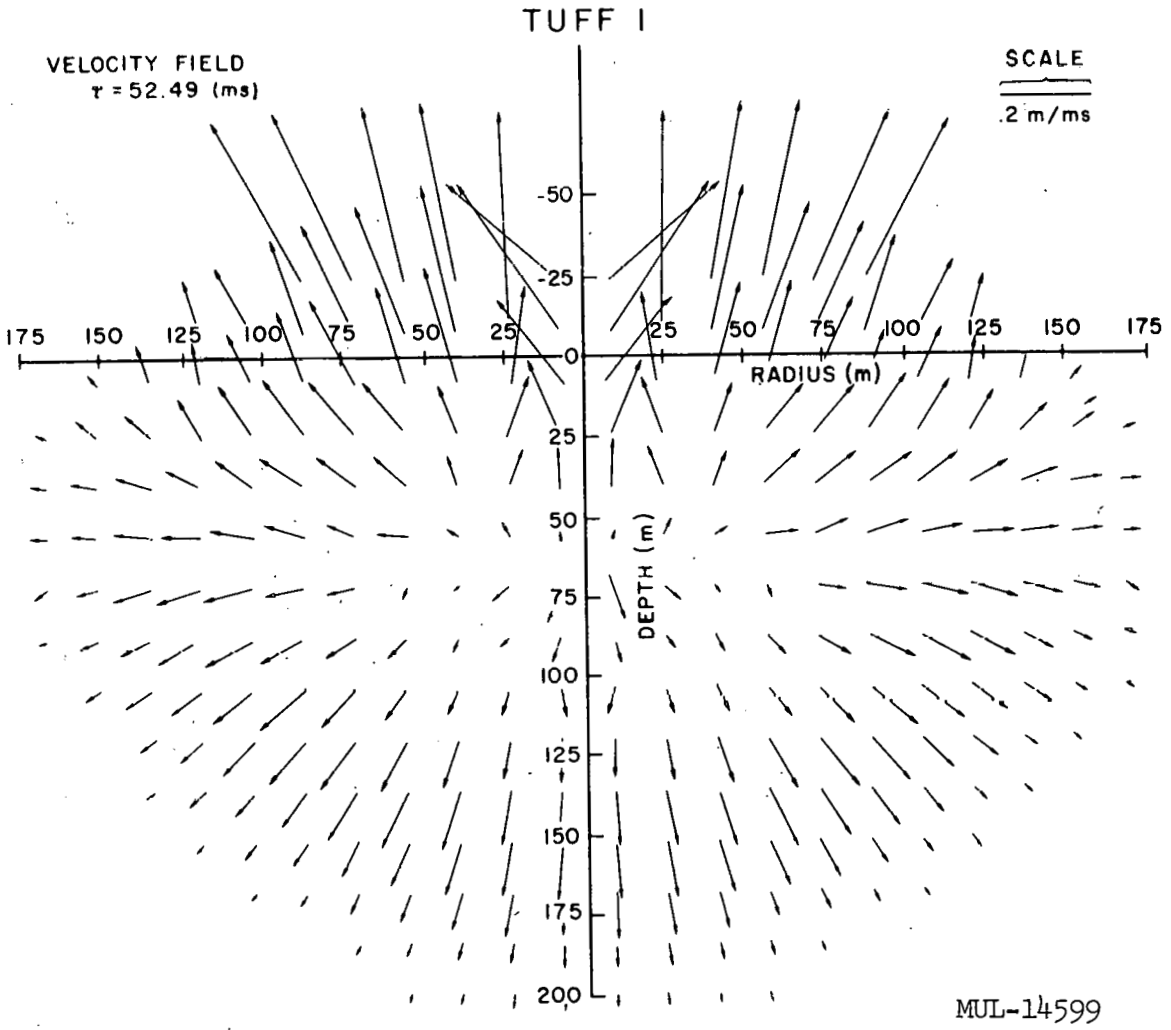
TUFF I
VELOCITY FIELD
τ = 52.49 (ms)
SCALE
.2 m/ms
-50
-25
175 150 125 100 75 50 25
0
25 50 75 100 125 150 175
RADIUS (m)
25
50
75
100
125
150
175
200
DEPTH (m)
MUL-14599

Fig. 10

TUFF I

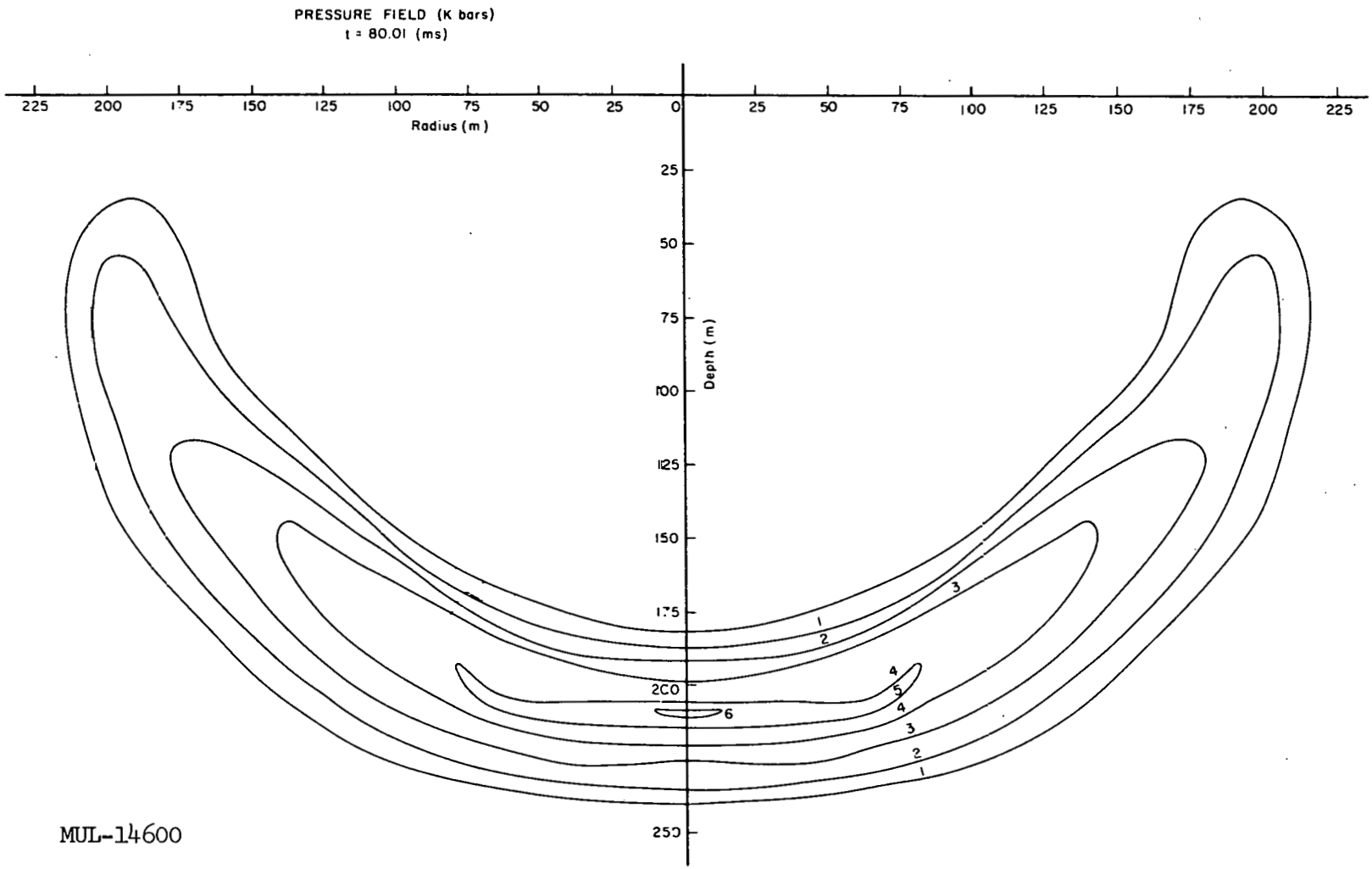
PRESSURE FIELD (K bars)
t = 80.01 (ms)
225 200 175 150 125 100 75 50 25 0 25 50 75 100 125 150 175 200 225
Radius (m)
25
50
75
100
125
150
175
200
250
Depth (m)
1
2
3
4
5
6
MUL-14600

Fig. 11

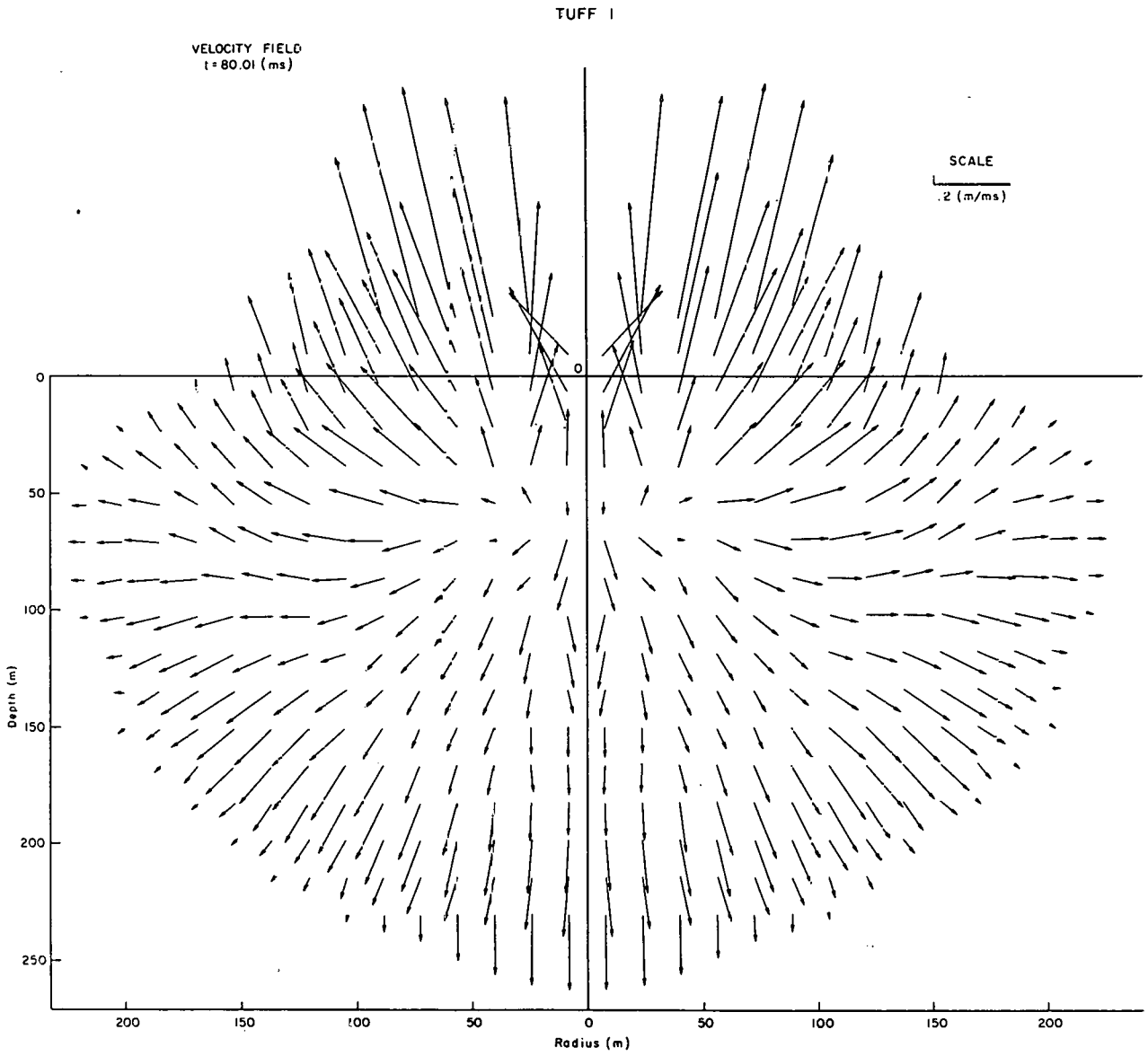

MUL-14601

Fig. 12

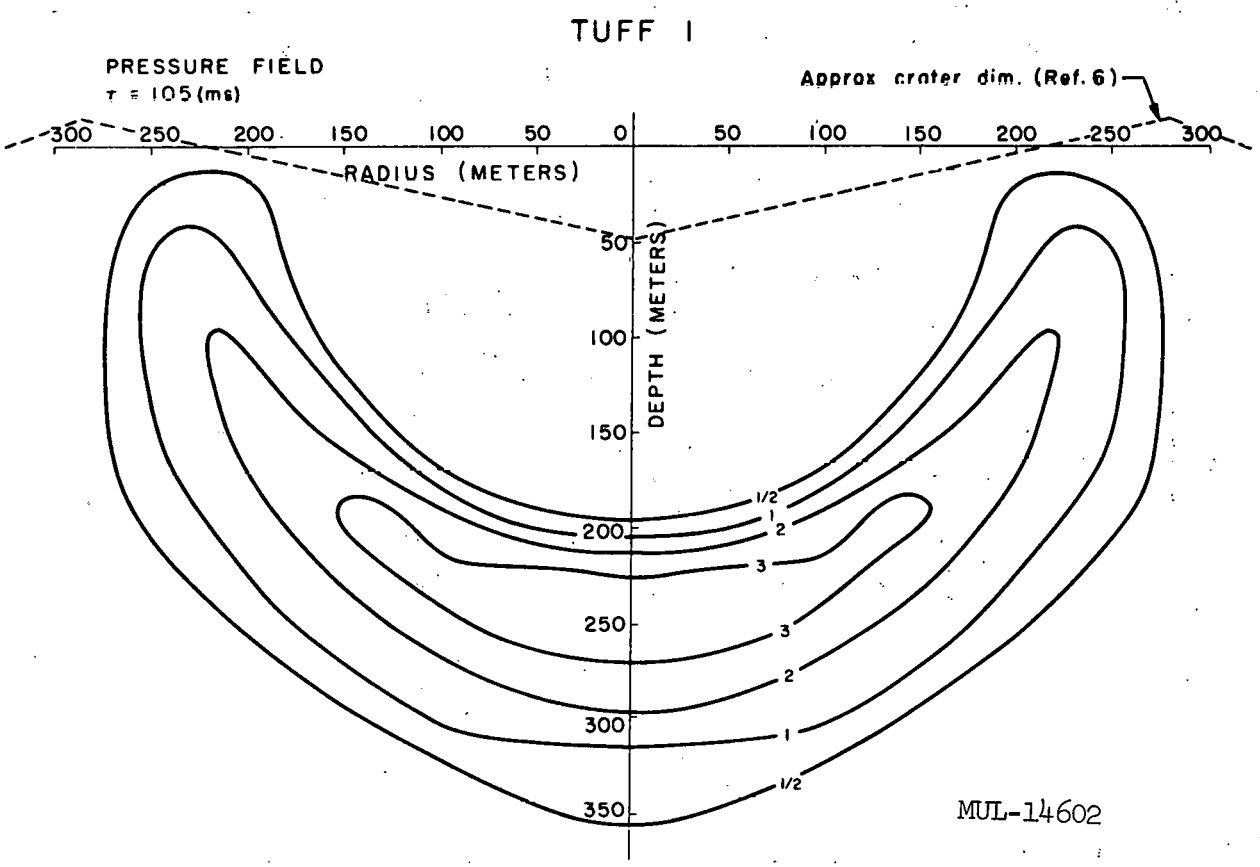
TUFF I
PRESSURE FIELD
τ = 105 (ms)
Approx crater dim. (Ref. 6)
300 250 200 150 100 50 0 50 100 150 200 250 300
RADIUS (METERS)
DEPTH (METERS)
50
100
150
200
250
300
350
1/2
1
2
3
3
2
1
1/2
MUL-14602

Fig. 13

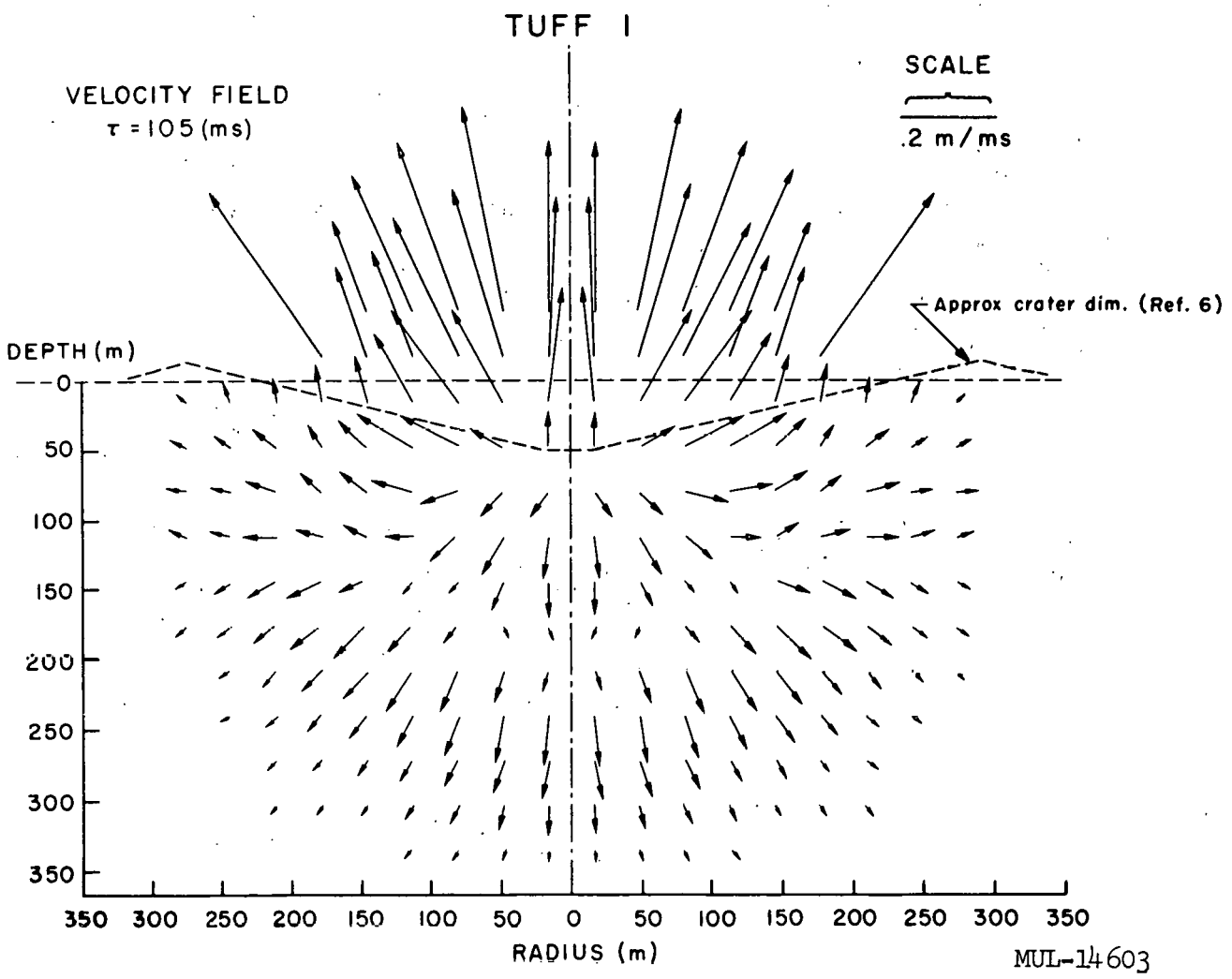
TUFF I
VELOCITY FIELD
τ = 105 (ms)
SCALE
.2 m/ms
Approx crater dim. (Ref. 6)
DEPTH (m)
0
50
100
150
200
250
300
350
350 300 250 200 150 100 50 0 50 100 150 200 250 300 350
RADIUS (m)
MUL-14603

Fig. 14

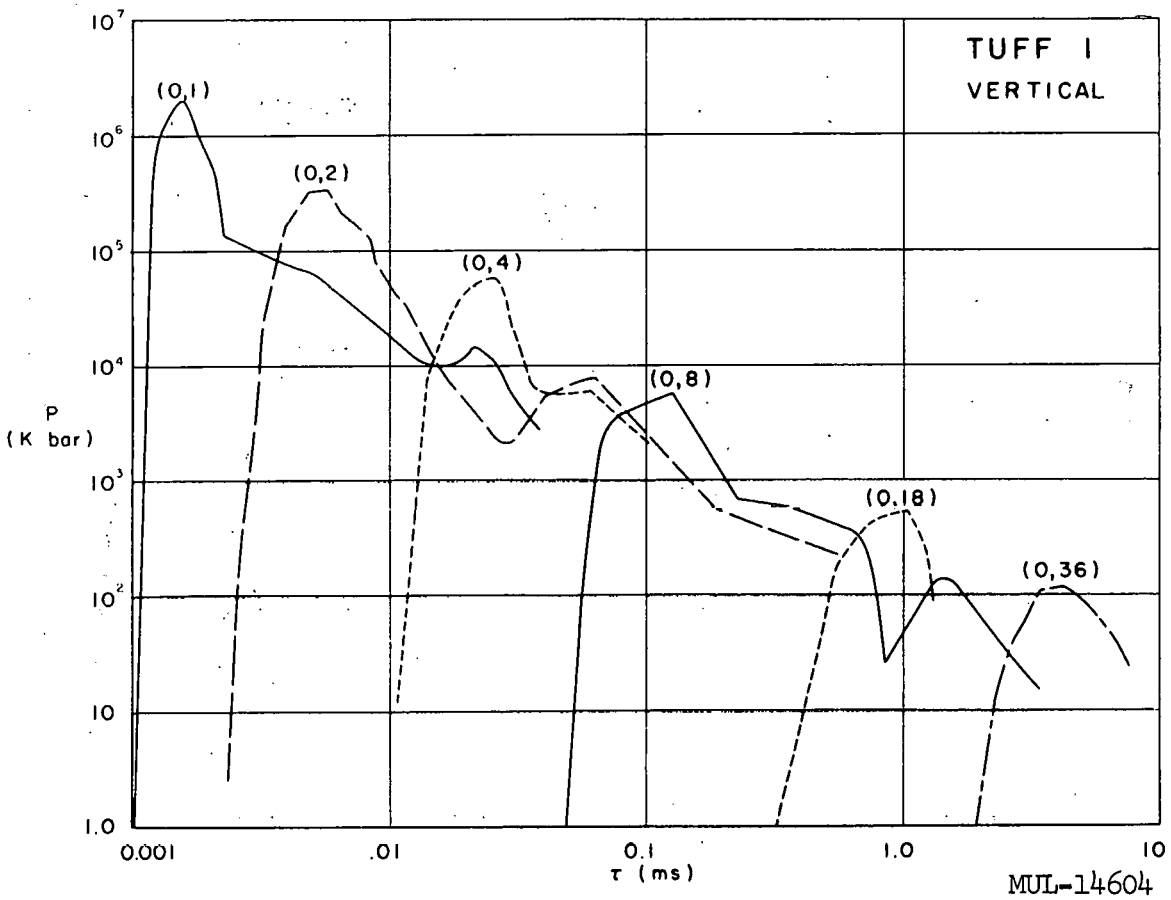

Fig. 15 — Pressure vs time at indicated depths (m) below burst point

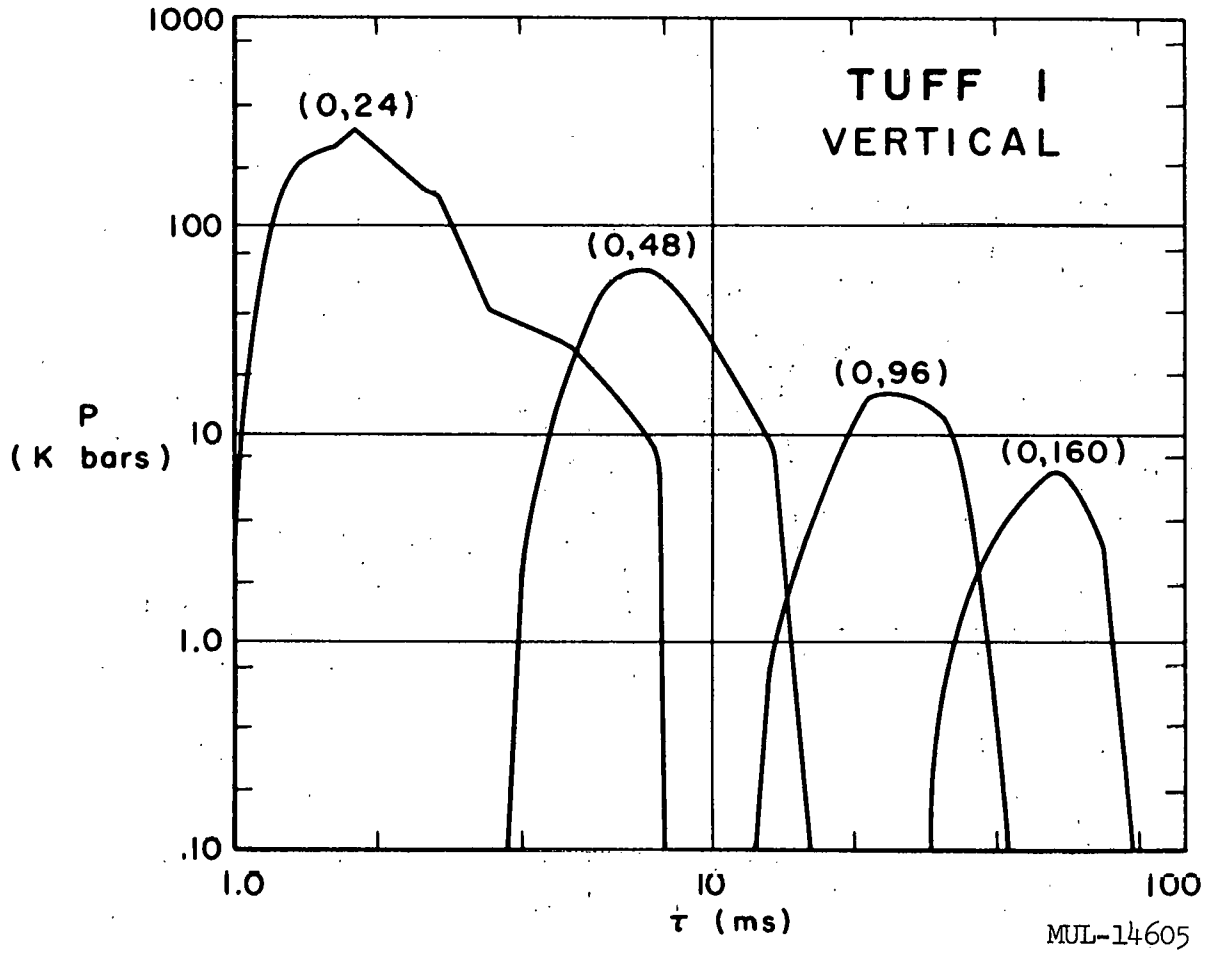

Fig. 16—Pressure vs time at indicated depths (m) below burst point

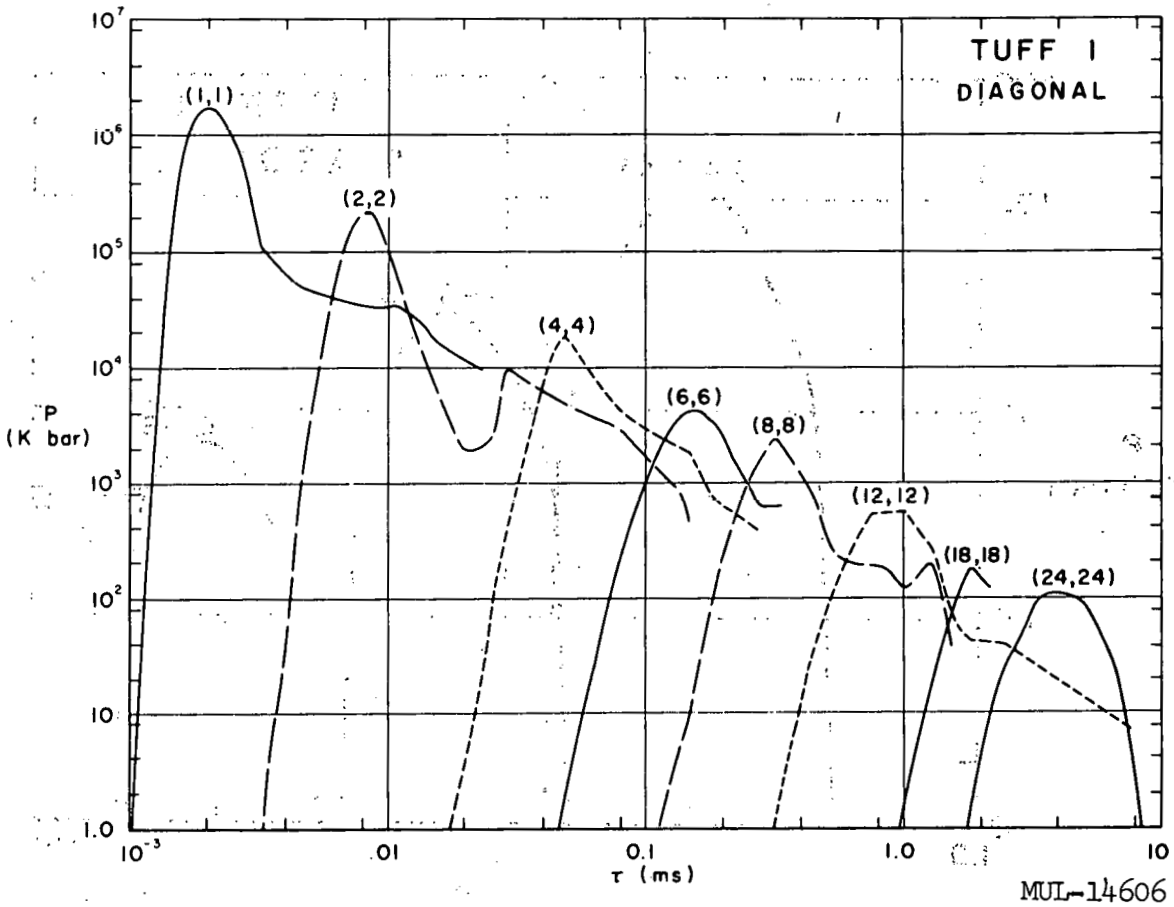

Fig. 17 — Pressure vs time at points with radii and depths indicated in meters

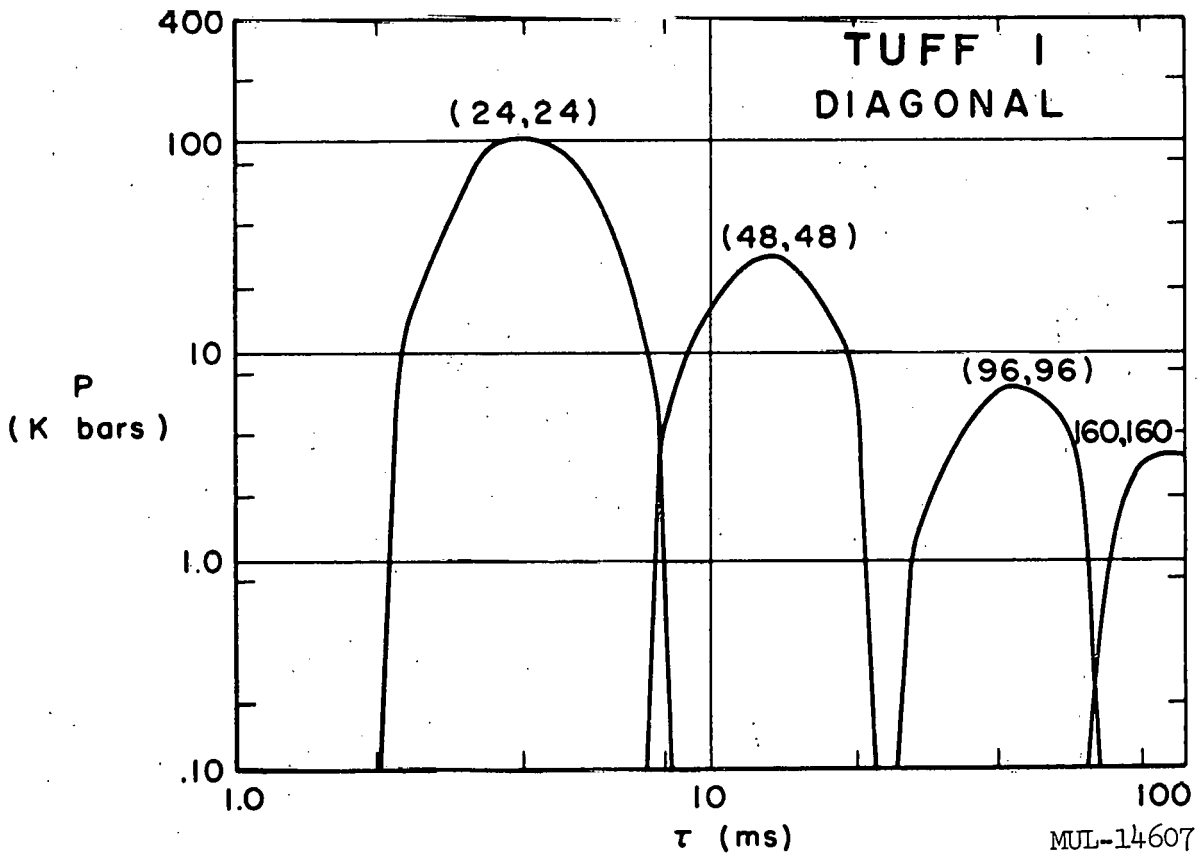

Fig. 18—Pressure vs time at indicated positions (m)

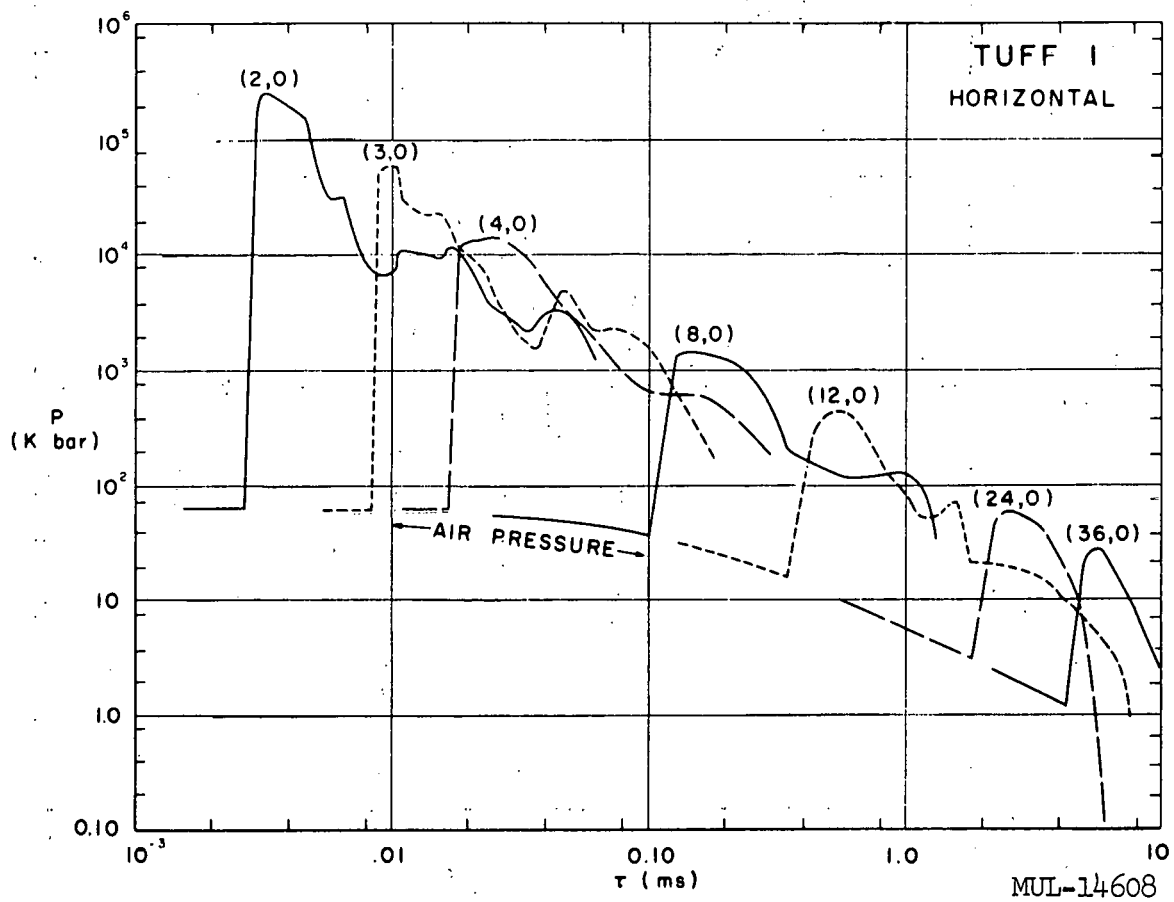

Fig. 19 — Pressure vs time at indicated radial distances (m) at the surface

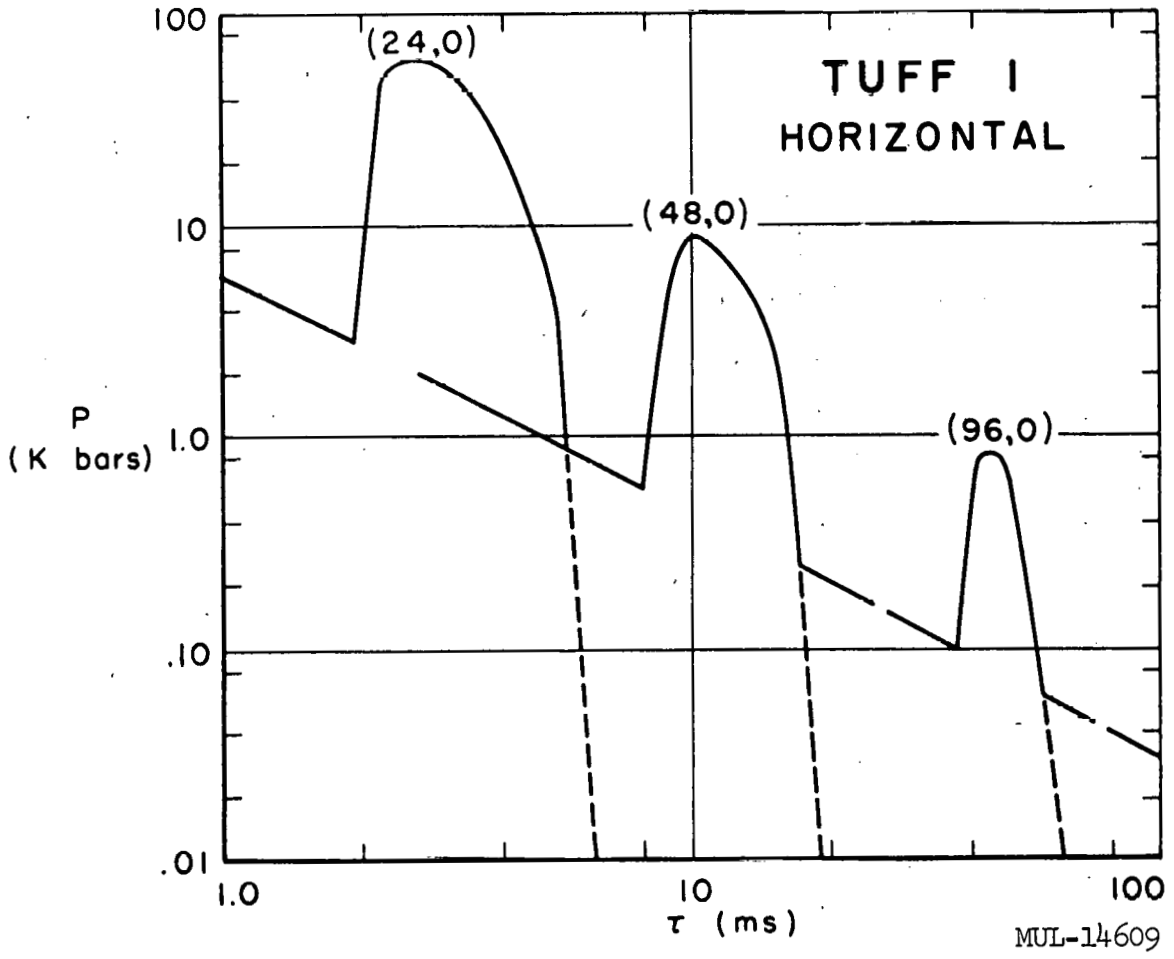

Fig. 20—Pressure vs time at indicated radii (m) along the surface

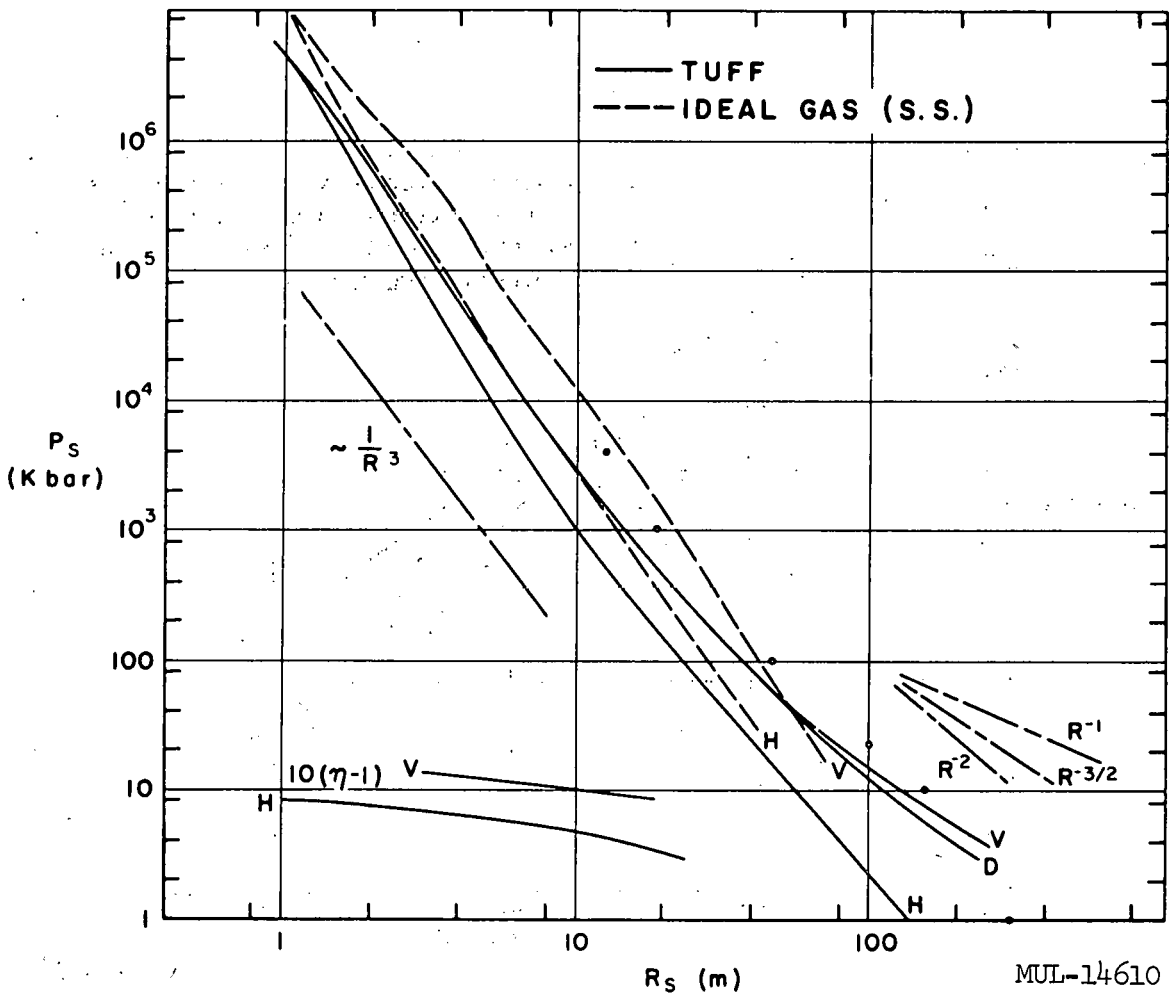

Fig. 21—Peak pressures and compressions (η-1) vs range along vertical (V), horizontal (H), and diagonal (D), from burst point

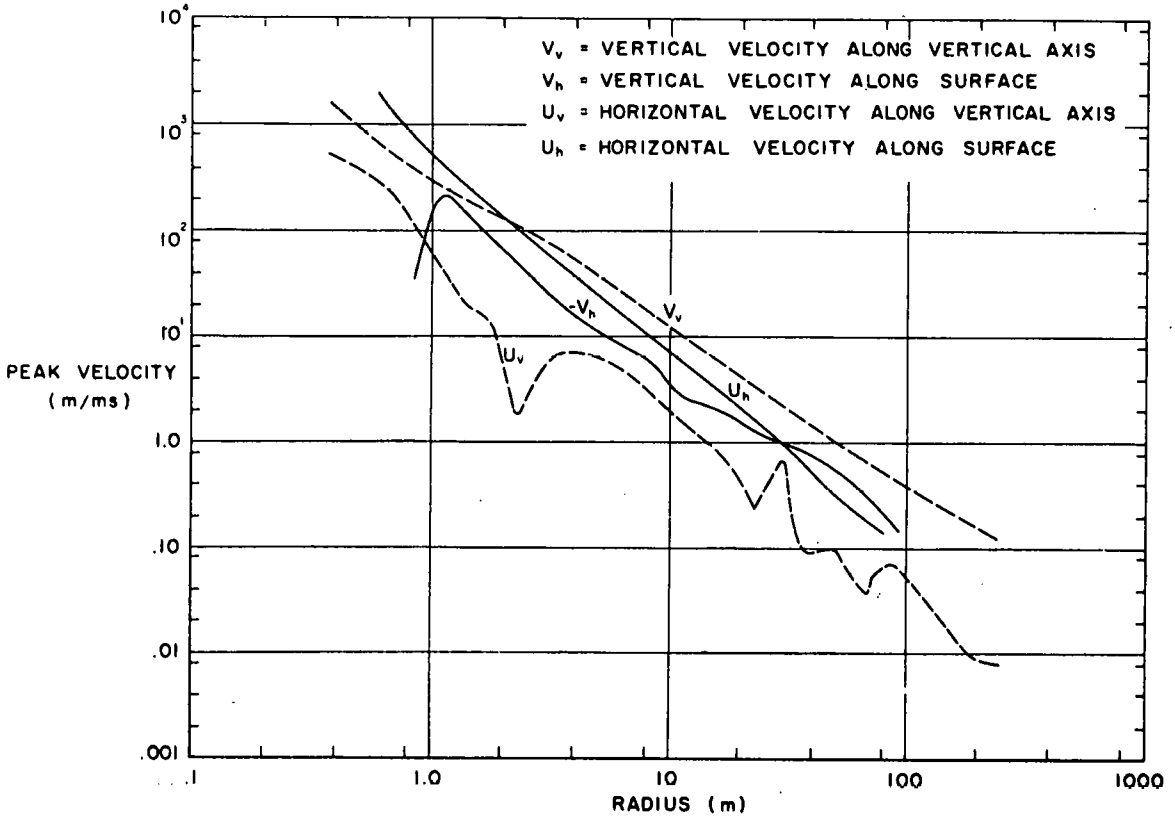

MUL-14611

Fig. 22

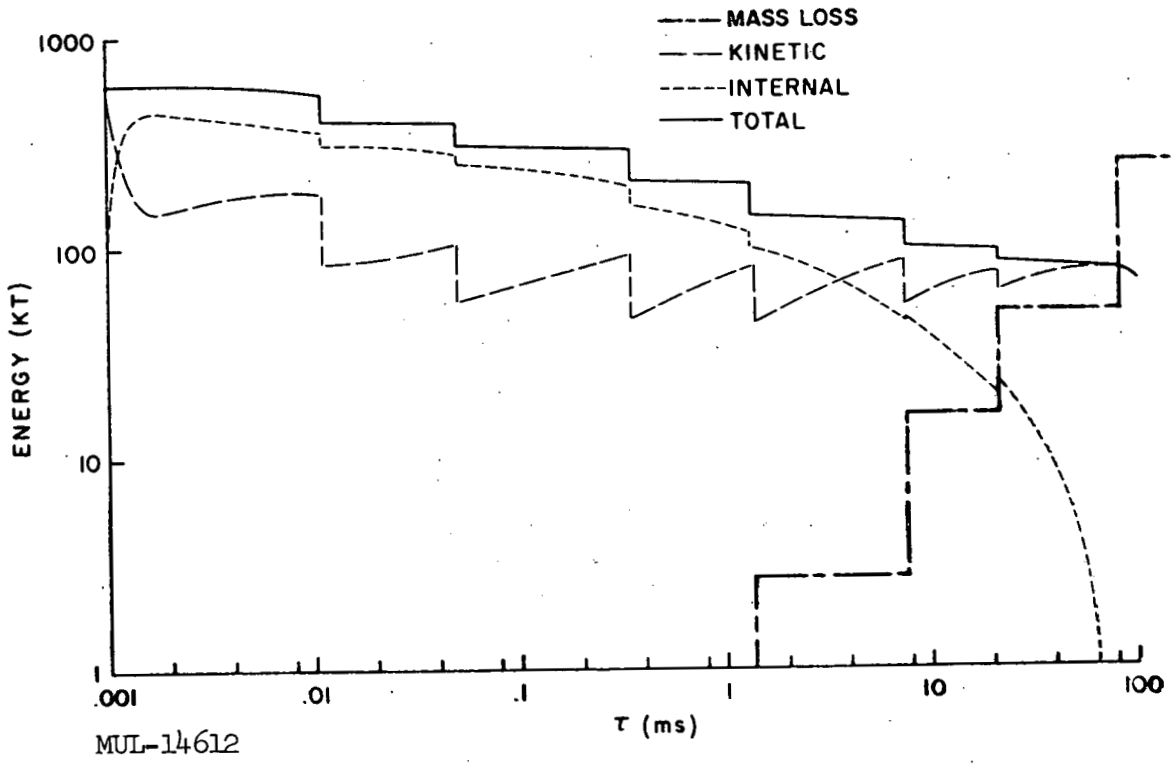

Fig. 23 — Energies and mass loss vs time